ZU-TH 27/18, CERN-TH-2018-167

Higgs boson production at the LHC using the q_T subtraction formalism at N^{3}LO QCD

Leandro Cieri[(a,b)], **Xuan Chen**[(b)], **Thomas Gehrmann**[(b)], **E.W.N. Glover**[(c)] **and Alexander Huss**[(d)]

[(a)] INFN, Sezione di Milano-Bicocca, Piazza della Scienza 3, I-20126 Milano, Italy

[(b)] Physik-Institut, Universität Zürich, CH-8057 Zurich, Switzerland

[(c)] Institute for Particle Physics Phenomenology, Durham University, Durham, DH1 3LE, UK

[(d)] Theoretical Physics Department, CERN, 1211 Geneva 23, Switzerland

Abstract

We consider higher-order QCD corrections to Higgs boson production through gluon–gluon fusion in the large top quark mass limit in hadron collisions. We extend the transverse-momentum (q_T) subtraction method at the next-to-next-to-next-to-leading order (N^{3}LO) and combine it with the NNLO Higgs-plus-jet calculation to numerically compute differential infrared-safe observables at N^{3}LO for Higgs boson production in gluon fusion. To cancel the infrared divergences, we exploit the universal behaviour of the associated q_T distributions in the small-q_T region. We document all the necessary ingredients of the transverse-momentum subtraction method up to N^{3}LO. The missing third-order collinear functions, which contribute only at $q_T = 0$, are approximated using a prescription which uses the known result for the total Higgs boson cross section at this order. As a first application of the third-order q_T subtraction method, we present the N^{3}LO rapidity distribution of the Higgs boson at the LHC.

1 Introduction

The most straightforward and successful (as well as systematically improvable) approach to calculations for processes at high-momentum scales M in QCD is a perturbative expansion in the strong coupling $\alpha_s(M^2)$. Cross sections are written as a series expansion in the parameter α_s and an improvement in accuracy is obtained by calculating an increasing number of coefficients in the series. Until a few years ago, the standard for such calculations was next-to-leading order (NLO) accuracy. Recent years have seen a number of next-to-next-to-leading order (NNLO) results for many important processes of interest, such that the emerging standard for precision calculations relevant for LHC phenomenology is the second non-trivial order in the strong coupling α_s.

Reducing the theoretical uncertainties was one of the main motivations for the extension from NLO to NNLO accuracy. This is particularly relevant in two distinct situations. Firstly, NNLO corrections are mandatory for those processes where NLO corrections are comparable in size to the leading order (LO) contribution, both to establish the convergence of the perturbative expansion and to obtain reliable predictions. Secondly, benchmark processes that are measured with high experimental precision require equally precise theoretical preditions, otherwise the extraction of precise information about Standard-Model (SM) couplings or parton-distribution functions would be limited by the accuracy of the theoretical calculation rather than by the measurement.

Pushing the perturbative accuracy of QCD calculations to one order higher, implies developing new methods and techniques to achieve the cancellation of infrared (IR) divergences that appear at intermediate steps of the calculations. The past few years have witnessed a great development in NNLO subtraction prescriptions. The transverse momentum (q_T) subtraction method [1, 2, 3], the N-jettiness subtraction [4, 5], projection-to-Born [8], residue subtraction [6, 7], and the antenna subtraction method [9] have all been successfully used for LHC phenomenology.

However, in view of the impressive and continuously increasing quality of the measurements performed at LHC, in some cases NNLO accuracy is simply not enough to fully describe the LHC data. Typically, these are processes in which the size of the NLO corrections were comparable with the LO, and where the NNLO corrections still presented large modifications such that the size of the theoretical uncertainties remained larger than the experimental uncertainties.

This motivated a new theoretical effort to go beyond NNLO to include the next perturbative order: the next-to-next-to-next-to-leading order (N^{3}LO). Sum rules, branching fractions [10] and deep inelastic structure functions [11] have been known to this order for quite some time. At present, the only hadron collider observables for which N^{3}LO QCD corrections have been calculated are the total cross section for Higgs boson production in gluon fusion [12, 13] and in vector boson fusion [14]. First steps have been taken towards more differential observables by computing the first N^{3}LO threshold expansion terms to the Higgs boson rapidity distribution in gluon fusion [15]. Moreover, the projection-to-Born method has been most recently extended to compute differential distributions to N^{3}LO, with a proof-of-principle calculation [16] of jet production in deep inelastic scattering.

In this paper, we present the generalisation of the q_T subtraction method at N^{3}LO and use it to compute Higgs boson production differentially in the Higgs boson rapidity at N^{3}LO accuracy. The paper is organized as follows: in Sec. 2 we recall briefly the main ideas of the q_T subtraction formalism and we present the necessary ingredients up to N^{3}LO, specifying which

elements are known analytically and identifying the missing coefficients at N^{3}LO. In Sec. 3 we present a prescription for approximating the missing collinear functions at N^{3}LO based on the unitarity property of the integral of the transverse momentum distribution. In Sec. 4, we apply the q_T subtraction formalism at N^{3}LO to produce differential distributions in the rapidity of the Higgs boson. To validate our approach, Sec. 4.1 quantifies the quality of the approximations by repeating them at NNLO, where all of the ingredients to q_T subtraction are known. We assess the magnitude of different sources of systematic uncertainties at N^{3}LO in Sec. 4.2, yielding final results for the N^{3}LO Higgs boson rapidity distribution and the associated theoretical uncertainty in Sec. 4.3. Finally, in Sec. 5 we summarize our results.

2 The q_T subtraction formalism at N^{3}LO

This section is devoted to the generalisation of the transverse-momentum subtraction formalism to N^{3}LO in perturbative QCD. The method is illustrated in its general form and special attention is paid to the case of Higgs boson production through gluon–gluon fusion. The q_T subtraction formalism presented in this section is the third order extension of the subtraction method originally proposed in Refs. [1, 2, 3].

We consider the inclusive hard-scattering reaction

$$h_1(p_1) + h_2(p_2) \to F(\{q_i\}) + X \,, \tag{1}$$

where h_1 and h_2 are the two hadrons which collide with momenta p_1 and p_2 producing the identified colourless final-state system F, accompanied by an arbitrary and undetected final state X. The colliding hadrons have centre–of–mass energy $\sqrt{s}$, and are treated as massless particles ($s = (p_1 + p_2)^2 = 2p_1 \cdot p_2$). The observed final state F consists of a generic system of non-QCD partons composed of *one* or *more* colour singlet particles (such as vector bosons, photons, Higgs bosons, Drell–Yan (DY) lepton pairs and so forth) with momenta q_i^μ ($i = 3, 4, 5, \dots$). The total momentum of the system F is denoted by q^μ ($q = \sum_i q_i$) and it can be expressed in terms of the total invariant mass M ($q^2 = M^2$), the transverse momentum $\mathbf{q}_T$ with respect to the direction of the colliding hadrons, and the rapidity y ($2y = \ln(p_2 \cdot q / p_1 \cdot q)$) in the centre–of–mass system of the collision. Since F is colourless, the LO partonic Born cross section can be either initiated by $q\bar{q}'$ annihilation, as in the case of the Drell–Yan process, or by gluon–gluon fusion, as in the case of Higgs boson production.

In order to explain the basic idea of the subtraction formalism, we first notice that at LO, the transverse momentum $\mathbf{q}_T = \sum_i \mathbf{q}_{T\,i}$ of the final state system F is identically zero. Therefore, as long as $q_T \neq 0$, the N^{n}LO QCD contributions (with $n = 1, 2, 3$) are given by the N^{n-1}LO QCD contributions to the F+jet(s) final state. Consequently, if $q_T \neq 0$ we have:

$$\mathrm{d}\sigma^F_{\mathrm{N^nLO}}(q_T \neq 0) \equiv \mathrm{d}\sigma^{F+\mathrm{jets}}_{\mathrm{N^{n-1}LO}} \quad \text{with} \quad n = 1, 2, 3 \,. \tag{2}$$

The notation N^{n}LO stands for: N^{0}LO=LO, N^{1}LO=NLO, N^{2}LO=NNLO and so forth. Equation (2) implies that if $q_T \neq 0$ the infrared (IR) divergences that appear in the computation of $\mathrm{d}\sigma^F_{\mathrm{N^nLO}}(q_T \neq 0)$ are those already present in $\mathrm{d}\sigma^{F+\mathrm{jets}}_{\mathrm{N^{n-1}LO}}$. Therefore, provided that the IR singularities involved in $\mathrm{d}\sigma^F_{\mathrm{N^nLO}}(q_T \neq 0)$ can be handled and cancelled with the available subtraction methods at N^{n-1}LO, the only remaining singularities at N^{n}LO are associated with the limit $q_T \to 0$ and

we treat them with the transverse momentum subtraction method. Since the small-q_T behaviour of the transverse momentum distribution is well known through the resummation program [17] of logarithmically-enhanced contributions to transverse-momentum distributions, we exploit this knowledge to construct the necessary N^{n}LO counterterms (CT) to subtract the remaining singularity at $q_T = 0$, thereby promoting the q_T subtraction method proposed in Refs. [1, 2, 3] to N^{n}LO.

The generic form of the q_T subtraction method [1] for the N^{n}LO cross section is

$$\mathrm{d}\sigma^F_{\mathrm{N^nLO}} = \mathcal{H}^F_{\mathrm{N^nLO}} \otimes \mathrm{d}\sigma^F_{\mathrm{LO}} + \left[\mathrm{d}\sigma^{F+\mathrm{jets}}_{\mathrm{N^{n-1}LO}} - \mathrm{d}\sigma^{F\,\mathrm{CT}}_{\mathrm{N^nLO}}\right] \quad \text{with} \quad n = 1, 2, 3\,, \tag{3}$$

where $\mathrm{d}\sigma^{F\,\mathrm{CT}}_{\mathrm{N^nLO}}$ is the contribution of the counterterm to the N^{n}LO cross section which cancels the divergences of $\mathrm{d}\sigma^{F+\mathrm{jets}}_{\mathrm{N^{n-1}LO}}$ in the limit $q_T \to 0$ and renders the term in square brackets finite for all values of q_T. The nth-order counterterm can be written

$$\mathrm{d}\sigma^{F\,\mathrm{CT}}_{\mathrm{N^nLO}} = \Sigma^F_{\mathrm{N^nLO}}(q_T^2/M^2)\ \mathrm{d}^2\mathbf{q}_T \otimes \mathrm{d}\sigma^F_{\mathrm{LO}}\,, \tag{4}$$

where the symbol $\otimes$ denotes convolutions over momentum fractions and sums over flavour indices of the partons. More precisely, the function $\Sigma^F_{\mathrm{N^nLO}}(q_T^2/M^2)$ is the nth-order truncation of the perturbative series in α_s

$$\Sigma^F_{c\bar{c}\leftarrow ab}\left(\frac{q_T^2}{M^2}; \frac{M^2}{\hat{s}}; \alpha_\mathrm{s}; \frac{M^2}{\mu_R^2}, \frac{M^2}{\mu_F^2}\right) = \sum_{n=1}^{\infty}\left(\frac{\alpha_\mathrm{s}}{\pi}\right)^n \Sigma^{F;(n)}_{c\bar{c}\leftarrow ab}\left(\frac{q_T^2}{M^2}; \frac{M^2}{\hat{s}}; \frac{M^2}{\mu_R^2}, \frac{M^2}{\mu_F^2}\right)\,, \tag{5}$$

where the labels a and b stands for the partonic channels of the N^{n}LO correction to the Born cross section ($\mathrm{d}\sigma^F_{\mathrm{LO}} \equiv \mathrm{d}\left[\sigma^{F;(0)}_{c\bar{c}}\right]$). Notice that at LO the only available configuration is $a = c$ and $b = \bar{c}$, where $c\bar{c}$ is (are) the partonic channel(s) through which the LO cross section is initiated. The function $\Sigma^F(q_T^2/M^2)$ embodies all the logarithmic terms that are divergent in the limit $q_T \to 0$ reproducing the singular behaviour of $\mathrm{d}\sigma^{F+\mathrm{jets}}$ in the small-q_T limit. The definition of the counterterm is free of terms proportional to $\delta(q_T^2)$ which are all absorbed in the perturbative factor $\mathcal{H}^F$. The hard coefficient function $\mathcal{H}^F_{\mathrm{N^nLO}}$ that encodes all the IR finite terms of the n-loop contributions, is obtained by the N^{n}LO truncation of the perturbative function

$$\mathcal{H}^F_{c\bar{c}\leftarrow ab}\left(\frac{M^2}{\hat{s}}; \alpha_\mathrm{s}; \frac{M^2}{\mu_R^2}, \frac{M^2}{\mu_F^2}\right) = \delta_{c\,a}\,\delta_{\bar{c}\,b}\,\delta(1-z) + \sum_{n=1}^{\infty}\left(\frac{\alpha_\mathrm{s}}{\pi}\right)^n \mathcal{H}^{F;(n)}_{c\bar{c}\leftarrow ab}\left(z; \frac{M^2}{\mu_R^2}, \frac{M^2}{\mu_F^2}\right)\,, \tag{6}$$

where $z = M^2/s$. According to the transverse momentum resummation formula (Eq. (10) of Ref. [2]) and using the Fourier-Bessel transformation between the conjugate variables q_T and the impact parameter b, the perturbative hard function $\mathcal{H}^F$ and the corresponding counterterm are obtained by the fixed-order truncation of the identity

$$\begin{aligned}\left(\Sigma^F_{c\bar{c}\leftarrow ab}\left(\frac{q_T^2}{M^2}; \frac{M^2}{\hat{s}}; \alpha_\mathrm{s}\right) + \mathcal{H}^F_{c\bar{c}\leftarrow ab}\left(\frac{M^2}{\hat{s}}; \alpha_\mathrm{s}\right)\right) \otimes \mathrm{d}\left[\sigma^{F;(0)}_{c\bar{c}}\right]_{ab} = \frac{M^2}{s}\int_0^\infty \mathrm{d}b\frac{b}{2}J_0(bq_T) \\ \times\, S_c(M,b)\int_{x_1}^1\frac{\mathrm{d}z_1}{z_1}\int_{x_2}^1\frac{\mathrm{d}z_2}{z_2}\mathrm{d}\hat{\sigma}^{F;(0)}_{c\bar{c}}\, f_{a/h_1}\left(x_1/z_1, b_0^2/b^2\right) f_{b/h_2}\left(x_2/z_2, b_0^2/b^2\right) \otimes \left[H^F C_1 C_2\right]_{c\bar{c};ab}\,,\end{aligned} \tag{7}$$

where $J_0(bq_T)$ is the 0th-order Bessel function, $f_{c/h}$ corresponds to the distribution of a parton c in a hadron h and $b_0 = 2e^{-\gamma_E}$ ($\gamma_E = 0.5772...$ is the Euler–Mascheroni constant). In the left hand side of Eq. (7), we omit the full scale dependence of these coefficients, which is however,

fully specified in Eqs. (5) and (6). The symbolic factor $\mathrm{d}\hat{\sigma}^{F;(0)}_{c\bar{c}}$ for the partonic Born cross section $\hat{\sigma}^{F;(0)}_{c\bar{c}}$ denotes

$$\mathrm{d}\hat{\sigma}^{F;(0)}_{c\bar{c}} \equiv \frac{\mathrm{d}\hat{\sigma}^{F;(0)}_{c\bar{c}}}{\mathrm{d}\phi} \; , \tag{8}$$

where ϕ represents the phase–space of the final state system F. In the left hand side of Eq. (7) the convolution (as well as sum over flavour indices of the partons) between the resummation functions $\Sigma^F_{c\bar{c}}$ and $\mathcal{H}^F_{c\bar{c}}$, the partonic Born cross section and the parton distributions is symbolically denoted by $\otimes d\left[\sigma^{F;(0)}_{c\bar{c}}\right]_{ab}$.

The large logarithmic corrections are exponentiated in the Sudakov form factor $S_c(M,b)$ of the quark ($c = q, \bar{q}$) or of the gluon ($c = g$), and it has the following expression:

$$S_c(M,b) = \exp\left\{ - \int_{b_0^2/b^2}^{M^2} \frac{\mathrm{d}q^2}{q^2} \left[A_c(\alpha_{\mathrm{s}}(q^2)) \; \ln\frac{M^2}{q^2} + B_c(\alpha_{\mathrm{s}}(q^2)) \right] \right\} \; . \tag{9}$$

The functions A and B in Eq. (9) permit a perturbative expansion in α_{s}:

$$A_c(\alpha_{\mathrm{s}}) \;=\; \sum_{n=1}^{\infty} \left(\frac{\alpha_{\mathrm{s}}}{\pi}\right)^n A_c^{(n)} \; , \tag{10}$$

$$B_c(\alpha_{\mathrm{s}}) \;=\; \sum_{n=1}^{\infty} \left(\frac{\alpha_{\mathrm{s}}}{\pi}\right)^n B_c^{(n)} \; . \tag{11}$$

The structure of the symbolic factor denoted by $\left[H^F C_1 C_2\right]_{c\bar{c};ab}$ in Eq.(7), depends on the initial state channel of the Born subprocess and is explained in detail in Refs. [19, 20]. Here we limit ourselves to the case in which the final state system F is composed of a single Higgs boson

$$\begin{aligned} \left[H^{F=H} C_1 C_2\right]_{gg;ab} \;&=\; H_g^{F=H}(\alpha_{\mathrm{s}}(M^2)) \; \left[\; C_{g\,a}(z_1;\alpha_{\mathrm{s}}(b_0^2/b^2)) \; C_{g\,b}(z_2;\alpha_{\mathrm{s}}(b_0^2/b^2)) \right. \\ &+\; \left. G_{g\,a}(z_1;\alpha_{\mathrm{s}}(b_0^2/b^2)) \; G_{g\,b}(z_2;\alpha_{\mathrm{s}}(b_0^2/b^2)) \; \right] \; . \end{aligned} \tag{12}$$

The right-hand side of Eq. (12) does not depend on the direction of $\mathbf{b}$ and this implies that the $\mathbf{q}_T$ distribution has no azimuthal correlations in the small-q_T region for Higgs boson production [19]. The presence of the $G_{g\,a}(z;\alpha_{\mathrm{s}})$ functions on the right-hand side of Eq. (12) is the manifestation of helicity-flip contributions. In Eq. (12), there are contributions with two $G_{g\,a}(z;\alpha_{\mathrm{s}})$ functions, since for Higgs boson production there can only be double helicity-flip terms: helicity conservation in the hard-process factor for Higgs boson production forbids contributions with a single helicity-flip. The helicity-flip $G_{g\,a}(z;\alpha_{\mathrm{s}})$ functions are absent in processes initiated at the Born level by quark annihilation [19]. The gluonic hard–collinear coefficient function $C_{g\,a}(z;\alpha_{\mathrm{s}})$ ($a = q, \bar{q}, g$) on the right-hand side of Eq. (12) has the following perturbative expansion

$$C_{g\,a}(z;\alpha_{\mathrm{s}}) = \delta_{g\,a} \; \delta(1-z) + \sum_{n=1}^{\infty} \left(\frac{\alpha_{\mathrm{s}}}{\pi}\right)^n C_{g\,a}^{(n)}(z) \; . \tag{13}$$

At variance with Eq. (13), the perturbative expansion of the coefficient functions G_{ga}, which are specific to gluon-initiated processes, starts only at $\mathcal{O}(\alpha_{\mathrm{s}})$, and can be written as [19, 20]

$$G_{g\,a}(z;\alpha_{\mathrm{s}}) = \sum_{n=1}^{\infty} \left(\frac{\alpha_{\mathrm{s}}}{\pi}\right)^n G_{g\,a}^{(n)}(z) \; . \tag{14}$$

The IR finite contribution of the n-loop correction terms to the Born subprocess are contained in the hard–virtual function

$$H_g^{F=H}(\alpha_{\rm s}) = 1 + \sum_{n=1}^{\infty} \left(\frac{\alpha_{\rm s}}{\pi}\right)^n H_g^{F=H\,;(n)} \quad . \tag{15}$$

We now turn to the discussion of the resummation scheme dependence of the coefficient functions. The resummation formula (7) is invariant under the following "resummation scheme" transformations [21]:

$$\begin{aligned} H_c^F(\alpha_{\rm s}) &\to H_c^F(\alpha_{\rm s})\ [\,h(\alpha_{\rm s})\,]^{-1}\ , \\ B_c(\alpha_{\rm s}) &\to B_c(\alpha_{\rm s}) - \beta(\alpha_{\rm s})\ \frac{d\ln h(\alpha_{\rm s})}{d\ln\alpha_{\rm s}}\ , \\ C_{ab}(\alpha_{\rm s},z) &\to C_{ab}(\alpha_{\rm s},z)\ [\,h(\alpha_{\rm s})\,]^{1/2}\ , \\ G_{ab}(\alpha_{\rm s},z) &\to G_{ab}(\alpha_{\rm s},z)\ [\,h(\alpha_{\rm s})\,]^{1/2}\ . \end{aligned} \tag{16}$$

The invariance can easily be proven by using the following renormalization-group identity:

$$h(\alpha_{\rm s}(b_0^2/b^2)) = h(\alpha_{\rm s}(M^2))\ \exp\left\{ -\int_{b_0^2/b^2}^{M^2} \frac{{\rm d}q^2}{q^2}\ \beta(\alpha_{\rm s}(q^2))\ \frac{{\rm d}\ln h(\alpha_{\rm s}(q^2))}{{\rm d}\ln\alpha_{\rm s}(q^2)} \right\}\ , \tag{17}$$

which is valid for any perturbative function $h(\alpha_{\rm s})$. Notice that Eq. (17) establishes the evolution of the perturbative functions from the scale $q^2 = b_0^2/b^2$ to $q^2 = M^2$. The QCD β-function and its corresponding nth-order β_n coefficient are defined as

$$\frac{{\rm d}\ln\alpha_{\rm s}(\mu^2)}{{\rm d}\ln\mu^2} = \beta(\alpha_{\rm s}(\mu^2)) = -\sum_{n=0}^{+\infty} \beta_n \left(\frac{\alpha_{\rm s}}{\pi}\right)^{n+1} \quad . \tag{18}$$

The explicit expression of the first three coefficients [22, 23], β_0, β_1 and β_2 are

$$\begin{aligned} &\beta_0 = \frac{1}{12}\left(11C_A - 2N_f\right)\ , \qquad \beta_1 = \frac{1}{24}\left(17C_A^2 - 5C_AN_f - 3C_FN_f\right)\ , \\ &\beta_2 = \frac{1}{64}\left(\frac{2857}{54}C_A^3 - \frac{1415}{54}C_A^2N_f - \frac{205}{18}C_AC_FN_f + C_F^2N_f + \frac{79}{54}C_AN_f^2 + \frac{11}{9}C_FN_f^2\right)\ , \end{aligned} \tag{19}$$

where N_f is the number of massless QCD flavours and the $SU(N_c)$ colour factors are $C_A = N_c$ and $C_F = (N_c^2-1)/(2N_c)$.

The physical origin of the resummation scheme invariance of Eq. (7) is discussed in Ref. [21]. The invariance implies that the hard–virtual factors H_c^F, S_c (more precisely, the function B_c contained in it) and C_{ab} are not unambiguously defined order-by-order in perturbation theory. After choosing a "resummation scheme", these factors can be unambiguously specified and computed. We rely on the *hard resummation scheme* defined in Ref. [20], which states all the contributions proportional to $\delta(1-z)$ are considered in the hard–virtual functions H_c^F. This directly implies that H_c^F is process dependent whereas the collinear C_{ab} functions and the resummation coefficients B_c are independent of the final state system F. In addition, the resummation coefficients A_c and the helicity-flip functions G_{ab} are also independent of the final state process.

The truncation of Eq. (7) at a given fixed order requires the explicit knowledge of resummation coefficients and hard collinear coefficient functions. For $F = H$ at NLO, the knowledge of the coefficients $A_g^{(1)}$, $B_g^{(1)}$, $C_{ga}^{(1)}$ $(a = q, \bar{q}, g)$ and $H_g^{H;(1)}$ are sufficient to compute the inclusive total cross section and differential distributions. Assuming that the Higgs boson couples to a single heavy quark of mass m_Q, the first-order coefficient $H_g^{H;(1)}$ in the hard scheme is [20]

$$H_g^{H;(1)} = C_A \pi^2/2 + c_H(m_Q)\,. \tag{20}$$

The function $c_H(m_Q)$, which depends on the NLO virtual corrections of the Born subprocess $\mathrm{d}\sigma_{\mathrm{LO}}^F$, is given in Eq. (B.2) of Ref. [36]. In the limit $m_Q \to \infty$, the function c_H becomes

$$c_H(m_Q) \longrightarrow \frac{5C_A - 3C_F}{2} = \frac{11}{2}\,. \tag{21}$$

Therefore the complete NLO set of coefficients necessary to compute Higgs boson production (in the limit in which the mass of the top quark $Q = t$ is larger than any other scale involved in the process) is

$$\begin{aligned} A_g^{(1)} &= C_A\,, \qquad B_g^{(1)} = -\frac{1}{6}\left(11C_A - 2N_f\right)\,, \qquad H_g^{H;(1)} = \frac{1}{2}(11 + C_A\pi^2)\,, \\ C_{ga}^{(1)}(z) &= \frac{1}{2}C_F\, z \qquad [a = q, \bar{q}]\,, \qquad C_{gg}^{(1)}(z) = 0\,. \end{aligned} \tag{22}$$

The coefficients $A_g^{(1)}$ and $B_g^{(1)}$ are process- as well as resummation scheme independent. In the hard resummation scheme the collinear functions $C_{ga}^{(1)}$ $(a = q, \bar{q}, g)$ are process independent, whereas $H_g^{H;(1)}$ depends on the final-state system $(F = H)$, and both depend on the resummation scheme in such a way to ensure the resummation scheme independence of Eq. (7) at NLO. The computation of the hard–virtual coefficients $H_c^{H;(1)}$ requires the definition of a specific prescription [24]. The explicit calculations and the results of Ref. [24] show that the NLO hard–virtual coefficient $H_c^{F;(1)}$ is explicitly related in a process-independent form to $\mathrm{d}\hat{\sigma}_{\mathrm{LO}}^F$ and to the IR finite part of the NLO virtual correction to the Born cross section. The previous process-independent relation is based on the definition of universal subtraction operators that cancel the IR divergences of the one-loop (NLO) virtual correction to the Born cross section and fix the first order IR finite constant δ_{q_T} [20]. The coefficient δ_{q_T}, which only depends on the initial-state partons, has a *soft* origin and it is defined in Refs. [24] and [20].

At NNLO, the coefficients $A_g^{(2)}$ and $B_g^{(2)}$ are needed [2, 20],

$$A_g^{(2)} = \frac{1}{2}\,C_A\left[\left(\frac{67}{18} - \frac{\pi^2}{6}\right)C_A - \frac{5}{9}N_f\right]\,, \qquad B_g^{(2)} = \frac{\gamma_g^{(1)}}{16} + \beta_0\, C_A\, \zeta_2\,, \tag{23}$$

where $\gamma_g^{(1)}$ is the coefficient of the $\delta(1-z)$ term in the NLO gluon splitting function [27, 28], which reads

$$\gamma_g^{(1)} = \left(-\frac{64}{3} - 24\zeta_3\right)C_A^2 + \frac{16}{3}\,C_A N_f + 4\,C_F N_f\,, \tag{24}$$

and ζ_n is the Riemann zeta-function for integer values n ($\zeta_2 = \pi^2/6$, $\zeta_3 = 1.202\ldots$, $\zeta_4 = \pi^4/90$). The coefficient $A_g^{(2)}$ does not depend on the resummation scheme whereas $B_g^{(2)}$ in Eq. (23) is valid in the hard resummation scheme and both coefficients are process independent. The collinear

functions $C_{ga}^{(2)}$ $(a = q, \bar{q}, g)$ in the hard resummation scheme can be extracted from Refs. [20, 25] and they are also independent of the final state system F.

The general structure of the hard–virtual coefficients H_c^F has been established only recently [20]. Although this factor is process dependent, Ref. [20] showed that H_c^F can be directly related in a universal (process independent) way to the IR finite part of the all-order virtual amplitude of the corresponding partonic subprocess $c\bar{c} \to F$. The precedent relation between H_c^F and the all-order virtual correction to the partonic subprocess $c\bar{c} \to F$ is explicitly known up to NNLO and it is based on the definition of universal subtraction operators that cancel the IR divergences of the two-loop (NNLO) virtual corrections to the Born cross section [30]. These universal second-order operators contain an IR finite term of soft origin ($\delta_{qT}^{(1)}$) that only depends on the initial-state partons [20].

In the case of Higgs-boson production, the hard–virtual factor $H_g^{F=H;(2)}$ in the large-m_t limit (in the hard scheme) is given by [25]

$$H_g^{H;(2)} = C_A^2 \left(\frac{3187}{288} + \frac{7}{8} L_t + \frac{157}{72}\pi^2 + \frac{13}{144}\pi^4 - \frac{55}{18}\zeta_3 \right) + C_A\, C_F \left(-\frac{145}{24} - \frac{11}{8} L_t - \frac{3}{4}\pi^2 \right) + \frac{9}{4} C_F^2 - \frac{5}{96} C_A - \frac{1}{12} C_F - C_A\, N_f \left(\frac{287}{144} + \frac{5}{36}\pi^2 + \frac{4}{9}\zeta_3 \right) + C_F\, N_f \left(-\frac{41}{24} + \frac{1}{2} L_t + \zeta_3 \right) , \tag{25}$$

where $L_t = \ln(M_H^2/m_t^2)$. The two-loop scattering amplitude [29] used in the computation of $H_g^{F=H;(2)}$ includes corrections to the large-m_t approximation. At NNLO, in Eq. (12) (which is proportional to $\delta(q_T^2)$) the first order $G_{ga}^{(1)}$ helicity-flip functions are required, they read [19]

$$G_{g\,a}^{(1)}(z) = C_a\, \frac{1-z}{z} \qquad\qquad a = q, \bar{q}, g\,, \tag{26}$$

where $C_{q;\bar{q}} = C_F$ and $C_g = C_A$. The first-order functions $G_{ga}^{(1)}$ are resummation-scheme independent and they do not depend on the final-state system F.

At N^{3}LO, the numerical implementation of Eq. (7) requires the following ingredients: $A_g^{(3)}$, $B_g^{(3)}$, $C_{ga}^{(3)}$, $G_{ga}^{(2)}$ $(a = q, \bar{q}, g)$ and $H_g^{H;(3)}$. The coefficient $A_g^{(3)}$ [40] reads

$$A_g^{(3)} = C_A^3 \left(\frac{245}{96} - \frac{67}{36}\zeta_2 + \frac{11}{24}\zeta_3 + \frac{11}{20}\zeta_2^2 \right) + C_A C_F N_f \left(-\frac{55}{96} + \frac{1}{2}\zeta_3 \right) - C_A N_f^2 \frac{1}{108} + C_A^2 N_f \left(-\frac{209}{432} + \frac{5}{18}\zeta_2 - \frac{7}{12}\zeta_3 \right) + \beta_0 C_A^2 \left(\frac{101}{27} - \frac{7}{2}\zeta_3 \right) - \beta_0 C_A N_f \frac{14}{27}\,. \tag{27}$$

The explicit expression of the $B_c^{(3)}$ $(a = q, g)$ coefficients in the hard scheme can be computed from Refs. [37, 38]. In the particular case of the gluon channel we have

$$B_g^{(3)} = -\frac{2133}{64} + \frac{3029}{576} N_f - \frac{349}{1728} N_f^2 + \frac{109}{6}\pi^2 - \frac{283}{144}\pi^2 N_f + \frac{5}{108}\pi^2 N_f^2 - \frac{253}{160}\pi^4 + \frac{23}{240}\pi^4 N_f - \frac{843}{8}\zeta_3 + 2\zeta_3 N_f + \frac{1}{6}\zeta_3 N_f^2 + \frac{9}{4}\pi^2\zeta_3 + \frac{135}{2}\zeta_5\,. \tag{28}$$

The analytical form of the function $\Sigma^{F;(3)}$ in Eq. (5) can be obtained by expanding Eq. (7) to the corresponding matching order. The full analytical formula for Σ^F is resummation scheme

independent order by order in the strong coupling constant. Therefore, the logarithmic singular behaviour for Σ^F at $q_T \to 0$ at each given order in α_s does not depend on the resummation scheme, and can be validated against the behaviour of the fixed order results at small q_T. To fully account for the logarithmically enhanced terms at a given order requires a sufficient depth in the resummation prior to its fixed-order expansion in Eq. (5). Specifically, the LO Higgs boson q_T distribution receives singular contributions from up to NLL (next-to-leading-logarithm) resummation [31, 32], the NLO Higgs boson q_T distribution requires the expansion of NNLL resummation [33, 24], and the NNLO Higgs boson q_T distribution has been recently validated against the singular contributions from N^{3}LL resummation [34, 35].

The function $\mathcal{H}^{F;(3)}_{c\bar{c}\leftarrow ab}$ which is proportional to $\delta(q_T^2)$, contains the functions $H_c^{H;(3)}$, $C_{ga}^{(3)}$ and $G_{ga}^{(2)}$ that are only known in parts or not at all. Nevertheless, within the q_T subtraction formalism, $\mathcal{H}^{F;(3)}$ can be inferred for any hard-scattering process whose corresponding total cross section is known at N^{3}LO. This point is discussed in detail in the next section.

3 The Higgs boson total cross section at N^{3}LO

We start this section with some observations related to the hard-scattering function $\mathcal{H}^F_{c\bar{c}\leftarrow ab}$. This function is resummation-scheme independent, but it depends on the specific hard-scattering subprocess $c + \bar{c} \to F$. The coefficients $\mathcal{H}^{F;(n)}_{c\bar{c}\leftarrow ab}$ of the perturbative expansion in Eq. (6) can be determined by performing a perturbative calculation of the q_T distribution in the limit $q_T \to 0$. In right-hand side of Eq. (7), the function $\mathcal{H}^F$ controls the strict perturbative normalization of the corresponding total cross section (i.e. the integral of the total q_T distribution). This unitary-related property can be exploited to determine the coefficients $\mathcal{H}^{F;(n)}_{c\bar{c}\leftarrow ab}$ from the perturbative calculation of the total cross section. At the partonic level, the integral of the total q_T distribution in Eq. (3) results in the total cross section $\hat{\sigma}^{\rm tot}_{F\,ab}$,

$$\hat{\sigma}^{\rm tot}_{F\,ab}(M,\hat{s};\alpha_s(\mu_R^2),\mu_R^2,\mu_F^2) = \int_0^\infty {\rm d}q_T^2\, \frac{{\rm d}\hat{\sigma}_{F\,ab}}{{\rm d}q_T^2}(q_T,M,\hat{s};\alpha_s(\mu_R^2),\mu_R^2,\mu_F^2)\,. \tag{29}$$

Since the the hard-scattering function $\mathcal{H}^F_{c\bar{c}\leftarrow ab}$ is simply proportional to $\delta(q_T^2)$, we evaluate the q_T spectrum on right-hand side of Eq. (3) according to the following decomposition

$$\hat{\sigma}^{\rm tot}_{F\,ab} = \frac{M^2}{\hat{s}}\,\mathcal{H}^F_{ab} + \int_0^\infty {\rm d}q_T^2\, \frac{{\rm d}\hat{\sigma}^{\rm (fin.)}_{F\,ab}}{{\rm d}q_T^2}\quad, \tag{30}$$

where $d\hat{\sigma}^{\rm (fin.)}_{F\,ab}$ is directly related to the quantity in square bracket in the right-hand side of Eq. (3)

$$\frac{{\rm d}\hat{\sigma}^{\rm (fin.)}_{F\,ab}}{{\rm d}q_T^2} \equiv \left[\frac{{\rm d}\hat{\sigma}^{F+{\rm jets}}_{ab}}{{\rm d}q_T^2} - \frac{{\rm d}\hat{\sigma}^{F\,{\rm CT}}_{ab}}{{\rm d}q_T^2}\right]\,. \tag{31}$$

Considering Eqs. (7) and (12) it is possible to write $\mathcal{H}^H_{gg}$ in terms of the functions $C_{g\,a}(z_1;\alpha_s)$ and $G_{g\,a}(z_1;\alpha_s)$ (in the particular case $F = H$), neglecting the scale dependent terms which are all known analytically (i.e. considering $\mu_F = \mu_R = M$)

$$\mathcal{H}^H_{gg\leftarrow ab}(z;\alpha_s) \equiv H_g^H(\alpha_s)\int_0^1 {\rm d}z_1 \int_0^1 {\rm d}z_2\,\delta(z-z_1z_2)\Big[C_{g\,a}(z_1;\alpha_s)C_{g\,b}(z_2;\alpha_s) + G_{g\,a}(z_1;\alpha_s)G_{g\,b}(z_2;\alpha_s)\Big]\,. \tag{32}$$

This expression for $\mathcal{H}^F_{ab}$ was written requiring specifically $F = H$, since its form depends on the initial state of the Born subprocess (quark annihilation or gluon fusion). There are two differences between Eqs. (12) and (32). The first difference is due to the fact that the function $\mathcal{H}^H$ depends on the energy fraction z, since the right-hand side of Eq. (32) involves a convolution integral over the momentum fractions z_1 and z_2. The second difference concerns the scale of α_s: in the functions $H^H_g(\alpha_s), C(\alpha_s)$ and $G(\alpha_s)$ on the right-hand side of Eq. (32), the argument of α_s is set to the same value (this common scale is not explicitly denoted in Eq. (32). Owing to this feature, the process-dependent function $\mathcal{H}^H_{gg\leftarrow ab}$ is unambiguously defined (i.e., it is independent of the specification of the resummation scheme) [21]. The $\mathcal{H}^H$ function in Eq. (32) can be expanded perturbatively without approximation at any order in the strong coupling constant α_s. The perturbative expansion of the function $\mathcal{H}^H$ directly follows from Eqs. (13)–(15) and for the first-order and second-order contributions we have

$$\mathcal{H}^{H;(1)}_{gg\leftarrow ab}(z) = \delta_{g\,a}\,\delta_{g\,b}\,\delta(1-z)\,H^{H;(1)}_g + \delta_{g\,a}\,C^{(1)}_{g\,b}(z) + \delta_{g\,b}\,C^{(1)}_{g\,a}(z) \;\;, \tag{33}$$

$$\begin{aligned}\mathcal{H}^{H;(2)}_{gg\leftarrow ab}(z) &= \delta_{g\,a}\,\delta_{g\,b}\,\delta(1-z)\,H^{H;(2)}_g + \delta_{g\,a}\,C^{(2)}_{g\,b}(z) + \delta_{g\,b}\,C^{(2)}_{g\,a}(z) \\ &\quad + H^{H;(1)}_g \left(\delta_{g\,a}\,C^{(1)}_{g\,b}(z) + \delta_{g\,b}\,C^{(1)}_{g\,a}(z)\right) + \left(C^{(1)}_{g\,a} \otimes C^{(1)}_{g\,b}\right)(z) + \left(G^{(1)}_{g\,a} \otimes G^{(1)}_{g\,b}\right)(z) \;\;.\end{aligned} \tag{34}$$

In Eq. (34) and in the following, the symbol $\otimes$ denotes the convolution integral (i.e., we define $(g \otimes h)(z) \equiv \int_0^1 dz_1 \int_0^1 dz_2\, \delta(z - z_1 z_2)\, g(z_1)\, h(z_2)$). The new third-order contribution is given by

$$\begin{aligned}\mathcal{H}^{H;(3)}_{gg\leftarrow ab}(z) &= \delta_{g\,a}\,\delta_{g\,b}\,\delta(1-z)\,H^{H;(3)}_g + \delta_{g\,a}\,C^{(3)}_{g\,b}(z) + \delta_{g\,b}\,C^{(3)}_{g\,a}(z) \\ &\quad + \left(G^{(1)}_{g\,a} \otimes G^{(2)}_{g\,b}\right)(z) + \left(G^{(2)}_{g\,a} \otimes G^{(1)}_{g\,b}\right)(z) \\ &\quad + H^{H;(1)}_g \left(\delta_{g\,a}\,C^{(2)}_{g\,b}(z) + \delta_{g\,b}\,C^{(2)}_{g\,a}(z)\right) + H^{H;(2)}_g \left(\delta_{g\,a}\,C^{(1)}_{g\,b}(z) + \delta_{g\,b}\,C^{(1)}_{g\,a}(z)\right) \\ &\quad + \left(C^{(1)}_{g\,a} \otimes C^{(2)}_{g\,b}\right)(z) + \left(C^{(2)}_{g\,a} \otimes C^{(1)}_{g\,b}\right)(z) \\ &\quad + H^{H;(1)}_g \left(C^{(1)}_{g\,a} \otimes C^{(1)}_{g\,b}\right)(z) + H^{H;(1)}_g \left(G^{(1)}_{g\,a} \otimes G^{(1)}_{g\,b}\right)(z) \;.\end{aligned} \tag{35}$$

As stated in Sec. 2, the second-order helicity-flip functions $G^{(2)}_{g\,a}(z)$ and the third-order collinear functions $C^{(3)}_{g\,a}(z)$ are not known. In addition, the third-order hard–virtual coefficient $H^{H;(3)}_g$ is not fully determined. In the following, we describe a procedure to obtain an approximation to these missing contributions.

The relation in Eq. (30) is valid order-by-order in QCD perturbation theory. Once the perturbative coefficients of the fixed-order expansions of $\hat{\sigma}^{\rm tot}_{F\,ab}$, $\mathcal{H}^F_{ab}$ and $\mathrm{d}\hat{\sigma}^{(\rm fin.)}_{F\,ab}/\mathrm{d}q_T^2$ are all known, the relation (30) has to be regarded as an identity, which can be explicitly checked. Since the fixed-order truncation of $\mathrm{d}\hat{\sigma}^{(\rm fin.)}_{F\,ab}/\mathrm{d}q_T^2$ does not contain any contributions proportional to $\delta(q_T^2)$, $\left[\mathrm{d}\hat{\sigma}^{(\rm fin.)}_{F\,ab}/\mathrm{d}q_T^2\right]_{\rm NLO}$ does not explicitly depend on the coefficient $\mathcal{H}^{F;(1)}_{ab}$. Analogously, $\left[\mathrm{d}\hat{\sigma}^{(\rm fin.)}_{F\,ab}/\mathrm{d}q_T^2\right]_{\rm NNLO}$ does not explicitly depend on the coefficient $\mathcal{H}^{F;(2)}_{ab}$, and so forth. Therefore, Eq. (30) can be used to determine the N$^{\rm n}$LO coefficient $\mathcal{H}^{F;(n)}_{ab}$ from the knowledge of $\hat{\sigma}^{\rm tot}_{F\,ab}$ at N$^{\rm n}$LO and of $\mathrm{d}\hat{\sigma}^{(\rm fin.)}_{F\,ab}/\mathrm{d}q_T^2$ at N$^{\rm n}$LO, without the need of explicitly computing the small-q_T behaviour of the spectrum $\mathrm{d}\hat{\sigma}_{F\,ab}/\mathrm{d}q_T^2$

at N$^{\rm n}$LO. For example, the N^{3}LO term in Eq. (30) reads

$$\left(\frac{\alpha_{\rm s}}{\pi}\right)^3 \; \frac{M^2}{\hat{s}} \sum_c \sigma^{(0)}_{c\bar{c},\,F}(\alpha_{\rm s}, M)\; \mathcal{H}^{F\,;(3)}_{c\bar{c}\leftarrow ab}\left(\frac{M^2}{\hat{s}}; \frac{M^2}{\mu_R^2}, \frac{M^2}{\mu_F^2}\right)$$
$$= \left\{ \left[\hat{\sigma}^{\rm tot}_{F\,ab}\right]_{\rm N^3LO} - \left[\hat{\sigma}^{\rm tot}_{F\,ab}\right]_{\rm NNLO} \right\} - \int_0^\infty {\rm d}q_T^2 \left\{ \left[\frac{{\rm d}\hat{\sigma}^{(\rm fin.)}_{F\,ab}}{{\rm d}q_T^2}\right]_{\rm N^3LO} - \left[\frac{{\rm d}\hat{\sigma}^{(\rm fin.)}_{F\,ab}}{{\rm d}q_T^2}\right]_{\rm NNLO} \right\} \quad , \tag{36}$$

where $\alpha_{\rm s} = \alpha_{\rm s}(\mu_R^2)$ and we have used

$$\left[\hat{\sigma}^{\rm tot}_{F\,ab}(M, \hat{s}; \alpha_{\rm s})\right]_{\rm LO} = \delta(1 - M^2/\hat{s}) \sum_c \sigma^{(0)}_{c\bar{c},\,F}(\alpha_{\rm s}, M)\; \delta_{ca}\; \delta_{\bar{c}b} \quad . \tag{37}$$

The generalization at any order $n > 1$ is [2]

$$\left(\frac{\alpha_{\rm s}}{\pi}\right)^n \; \frac{M^2}{\hat{s}} \sum_c \sigma^{(0)}_{c\bar{c},\,F}(\alpha_{\rm s}, M)\; \mathcal{H}^{F\,;(n)}_{c\bar{c}\leftarrow ab}\left(\frac{M^2}{\hat{s}}; \frac{M^2}{\mu_R^2}, \frac{M^2}{\mu_F^2}\right) \tag{38}$$
$$= \left\{ \left[\hat{\sigma}^{\rm tot}_{F\,ab}\right]_{\rm N^nLO} - \left[\hat{\sigma}^{\rm tot}_{F\,ab}\right]_{\rm N^{n-1}LO} \right\} - \int_0^\infty {\rm d}q_T^2 \left\{ \left[\frac{{\rm d}\hat{\sigma}^{(\rm fin.)}_{F\,ab}}{{\rm d}q_T^2}\right]_{\rm N^nLO} - \left[\frac{{\rm d}\hat{\sigma}^{(\rm fin.)}_{F\,ab}}{{\rm d}q_T^2}\right]_{\rm N^{n-1}LO} \right\} .$$

At LO, where only the Born subprocess is available, $\left[\frac{{\rm d}\hat{\sigma}^{(\rm fin.)}_{F\,ab}}{{\rm d}q_T^2}\right]_{\rm LO}$ is zero by definition. Notice that in Eqs. (36) and (38) the full $\mathcal{H}^{F\,;(n)}_{c\bar{c}\leftarrow ab}$ coefficient is used, i.e., the scale independent terms as well as the terms that we omitted in Eq. (32) (and therefore in Eqs. (33), (34) and (35) embody the scale dependence through the ratios M^2/μ_F^2 and M^2/μ_R^2.

If all the components on the right-hand side of Eq. (38) are known analytically (as it was the case at NNLO in Refs. [25, 26]) the function $\mathcal{H}^F_{ab}$ can be extracted exactly in analytical form. At NLO the extraction of the function $\mathcal{H}^{F\,;(1)}_{ab}$ is straightforward for Drell–Yan and Higgs boson production. The function $\mathcal{H}^{F\,;(2)}_{ab}$ at NNLO (for Higgs ($F = H$) boson production [25] and Drell–Yan ($F = DY$) [26]) can be obtained with a dedicated analytical computation using Eq. (38) for $n = 2$. Since for Higgs boson production, the transverse momentum cross section H+jet at NNLO is not known analytically, Eq. (36) can be used only numerically to compute $\mathcal{H}^{F\,;(3)}_{ab}$.

The following paragraphs will focus on the details of the approximation that we intend to use. Instead of computing the entire third-order function $\mathcal{H}^{H\,;(3)}_{ab}$ numerically, we first report all its ingredients with the aim of reducing the numerical extraction to only a few components (perturbative functions).

The general structure of the coefficient $\mathcal{H}^{F\,;(3)}$ (which is proportional to $\delta(q_T^2)$) is not known in analytic form for any hard-scattering process. Nonetheless, within the q_T subtraction formalism, $\mathcal{H}^{F\,;(3)}$ can be reliably approximated for any hard-scattering process whose corresponding total cross section is known at N^{3}LO.

At N^{3}LO, the universal relation between $H_c^{F;(3)}$ and the third-order virtual correction to the partonic subprocess $c\bar{c} \to F$ presents one missing ingredient: a *single* coefficient (of *soft* origin) belonging to the finite part of the structure of the IR singularities contained in the third-order virtual amplitude of the corresponding partonic subprocess $c\bar{c} \to F$. Although a general prescription

to compute the hard–virtual coefficient $H_g^{H;(3)}$ analytically is not fully known, using the corresponding hard–virtual factor $C_{gg\to H}^{\mathrm{th}(3)}$ [39] from threshold resummation (in the large-m_t limit) and the exponential equation that relates hard–virtual coefficients in threshold- and q_T-resummation (Eq. (81) of Ref. [20]), we compute the following approximate expression

$$\begin{aligned}
\widetilde{H}_g^{H;(3)} = C_A^3 \Bigg(& -\frac{15649\zeta_3}{432} - \frac{121\pi^2\zeta_3}{432} + \frac{3\zeta_3^2}{2} + \frac{869\zeta_5}{144} + \frac{215131}{5184} + \frac{16151\pi^2}{7776} - \frac{961\pi^4}{15552} + \frac{\pi^6}{810} \\
& + \frac{105}{32}\zeta_6 \Bigg) + C_A^2 \left(\frac{605\zeta_3}{72} + \frac{55\pi^2\zeta_3}{36} + \frac{737\pi^2}{432} + \frac{167\pi^4}{432} + \frac{\pi^6}{72} \right) \\
& + C_A \left(\frac{19\pi^2 L_t}{48} - \frac{55\pi^2\zeta_3}{8} - \frac{\pi^6}{480} + \frac{133\pi^4}{72} + \frac{11399\pi^2}{864} + \frac{63}{32}\zeta_6 \right) \\
& + N_f^2 \left(\frac{43 C_A \zeta_3}{108} - \frac{19\pi^4 C_A}{3240} - \frac{133\pi^2 C_A}{1944} + \frac{2515 C_A}{1728} - \frac{7 C_F \zeta_3}{6} \right. \\
& \left. + \frac{4481 C_F}{2592} - \frac{\pi^4 C_F}{3240} - \frac{23\pi^2 C_F}{432} \right) \\
& + N_f \left(\frac{101 C_A^2 \zeta_5}{72} - \frac{97}{216}\pi^2 C_A^2 \zeta_3 + \frac{29 C_A^2 \zeta_3}{8} + \frac{1849\pi^4 C_A^2}{38880} - \frac{35\pi^2 C_A^2}{243} - \frac{98059 C_A^2}{5184} \right. \\
& + \frac{5 C_A C_F \zeta_5}{2} + \frac{13 C_A C_F \zeta_3}{2} + \frac{1}{2}\pi^2 C_A C_F \zeta_3 - \frac{63991 C_A C_F}{5184} + \frac{11\pi^4 C_A C_F}{6480} - \frac{71}{216}\pi^2 C_A C_F \\
& + \frac{1}{9}\pi^2 C_A L_t - \frac{5}{36}\pi^2 C_A \zeta_3 - \frac{55 C_A \zeta_3}{36} - \frac{5\pi^4 C_A}{54} - \frac{1409\pi^2 C_A}{864} \\
& \left. - 5 C_F^2 \zeta_5 + \frac{37 C_F^2 \zeta_3}{12} + \frac{19 C_F^2}{18} \right) \, . \qquad (39)
\end{aligned}$$

Notice that we neglect all the third-order terms in the exponent of Eq. (81) in Ref. [20], considering the entire $\mathcal{O}(\alpha_{\mathrm{s}}^3)$ correction (in the exponent) as unknown. The $\widetilde{H}_g^{H;(3)}$ coefficient in Eq. (39) will be used in the numerical computations below.

The missing terms in Eq. (39), concerning the final expression of $H_g^{H;(3)}$, have a *soft* origin. Following the notation of Ref. [20], all the third-order terms in the right-hand side of Eq. (81) of Ref. [20] are denoted by $\delta_{(2)}^{q_T}$. This allows to perform a subsequent decomposition for the third-order hard–virtual coefficient defined in Eq. (39)

$$\widetilde{H}_g^{H;(3)} \equiv H_g^{H;(3)} - \left[H_g^{H;(3)} \right]_{(\delta_{(2)}^{q_T})} \, . \qquad (40)$$

Therefore the only missing ingredients to $H_c^{H;(3)}$ are the functions $G_{g\,a}^{(2)}(z)$, $C_{g\,a}^{(3)}(z)$ and $\left[H_g^{H;(3)} \right]_{(\delta_{(2)}^{q_T})}$. Their contribution to Eq. (36) can be approximated as follows:

$$\begin{aligned}
C_{N3} \;\; \delta_{g\,a}\,\delta_{g\,b}\,\delta(1-z) \;\; \leftarrow \;\; & \delta_{g\,a}\,\delta_{g\,b}\,\delta(1-z) \left[H_g^{H;(3)} \right]_{(\delta_{(2)}^{q_T})} + \delta_{g\,a}\, C_{g\,b}^{(3)}(z) + \delta_{g\,b}\, C_{g\,a}^{(3)}(z) \\
& + \left(G_{g\,a}^{(1)} \otimes G_{g\,b}^{(2)} \right)(z) + \left(G_{g\,a}^{(2)} \otimes G_{g\,b}^{(1)} \right)(z) \;\; , \qquad (41)
\end{aligned}$$

where the third-order numerical coefficient C_{N3} embodies the numerical extraction of the hard–virtual coefficient $\left[H_g^{H;(3)} \right]_{(\delta_{(2)}^{q_T})}$ *plus* the numerical approximation of a function of the variable z by a numerical term proportional to $\delta(1-z)$. The resulting numerical coefficient $\left[H_g^{H;(3)} \right]_{(\delta_{(2)}^{q_T})}$ is

exact since C_{N3} is proportional to $\delta(1-z)$. The approximation that implies Eq. (41) is related only to the functions $G_{g\,a}^{(2)}(z)$ and $C_{g\,a}^{(3)}(z)$, whose functional dependence on the variable z goes beyond terms proportional to $\delta(1-z)$.

The method outlined in Eq. (41) to approximate numerically unknown terms in the hard–virtual function $\mathcal{H}^{H}_{gg\leftarrow ab}(z)$ is not new. It was first used in Ref. [2] in order to compute the second-order function $\mathcal{H}^{H;(2)}_{gg\leftarrow ab}(z)$ numerically at NNLO, providing a reasonable estimate of the exact result to better than 1% accuracy. Notice that Eq. (41) allows to recover the total cross section (at N^{3}LO in this case) with no approximation. After integration over the transverse momentum q_T, Eq. (29) provides the same total integral (numerically in this case) as in the fully analytical case. Even more, for IR safe observables (at fixed order) which fulfil that the *back-to-back* kinematical region ($q_T = 0$) is located in a single phase space point (e.g. the q_T distribution, the angular separation $\Delta\Phi_{\gamma\gamma}$ between the two photons for a Higgs boson decaying into diphotons, etc.), the fixed-order result is also exact, i.e. the integral of the analytical unknown terms in Eq. (41) (which all have $q_T = 0$) is located in one single point of the exclusive differential distributions.

The previous considerations about the approximation that proposes Eq. (41) were regarding the total cross section or differential distributions in which the Born–like configurations belong to one single phase space point. In order to quantify the quality of the approximation proposed in Eq. (41) at the differential level even when the Born differential cross section populates the entire differential range, we perform a detailed numerical study of the Higgs boson rapidity y_H distribution in Sec. 4.1 at NNLO. Anticipating these results, we find that in the rapidity range $0 \leq y_H \leq 4$ the approximated NNLO result differs by less than 0.2% from the exact NNLO Higgs boson rapidity distribution.

3.1 Implementation and setup of the numerical calculations

To extract the value of C_{N3}, we first introduce the numerical tools and the calculational setup in this section. We use the same setup for the inclusive and differential predictions presented in Sections 3.2, 4.1, 4.2 and 4.3.

We consider Higgs boson production in proton–proton collisions at the centre-of-mass energy $\sqrt{s} = 13$ TeV. In our computation we use the Higgs boson mass $M_H = 125$ GeV and the vacuum expectation value $v = 246.2$ GeV. The Born subprocess is initiated with gluon–gluon fusion mediated through a top quark loop. For Higgs boson production, which has a typical energy scale of M_H, it is possible to integrate out the top quark loop by taking the large-m_t limit ($m_t \to \infty$) and therefore, the Higgs boson is produced from the gluon-gluon-Higgs boson effective vertex [41]. The mass of the top quark is taken as $m_t = 173.2$ GeV in those contributions which do not vanish in the large-m_t limit (e.g. Eqs. (25) and (39) and Wilson coefficient corrections at N^{3}LO). With the top quark loop replaced by an effective vertex, we consider a five-flavour scheme QCD with all light quarks being massless. We use the central set of the `PDF4LHC15` parton distribution functions (PDFs) [42] as implemented in the `LHAPDF` framework [43] and the associated strong coupling constant $\alpha_s(M_Z) = 0.118$. Notice that we systematically employ the same order of the PDFs (NNLO) for the LO, NLO, NNLO and N^{3}LO results presented in this paper. The default factorization and renormalization scales are chosen accordingly as $\mu \equiv \mu_R = \mu_F = M_H/2$. The theoretical uncertainty is estimated by varying the default scale choice independently for μ_R and

μ_F by a factor of $\{1/2, 2\}$ while omitting combinations of $\mu_R/\mu_F = 4$ or $1/4$ leading to seven-point scale variation choices.

As stated in Sec. 3 and in Refs. [1, 2], the computation of the total cross section or differential distributions with the q_T subtraction formalism can be separated into two main parts by inserting Eq. (31) into Eq. (30):

$$\hat{\sigma}^{\text{tot}}_{F\,ab} = \left[\frac{M^2}{\hat{s}}\,\mathcal{H}^F_{ab} - \int_0^\infty \mathrm{d}q_T^2\,\frac{\mathrm{d}\hat{\sigma}^{F\ \text{CT}}_{ab}}{\mathrm{d}q_T^2}\right] + \int_0^\infty \mathrm{d}q_T^2\,\frac{\mathrm{d}\hat{\sigma}^{F+\text{jets}}_{ab}}{\mathrm{d}q_T^2}\ . \tag{42}$$

Regarding the $\mathrm{d}\hat{\sigma}^{F+\text{jets}}_{ab}$ contribution in Eq. (42), we make use of the parton-level event generator `NNLOJET` which provides the necessary infrastructure for the antenna subtraction method up to NNLO [9]. This program performs the integration of all contributing subprocesses of the type $\mathrm{d}\hat{\sigma}^{F+\text{jets}}_{ab}$ as well as the convolution with PDFs at this order. Processes at NNLO with the structure of $\mathrm{d}\hat{\sigma}^{F+\text{jets}}_{ab}$ implemented in `NNLOJET` are: $F = H$ [44], $F = \gamma^*$, Z [45, 46] and $F = W^\pm$ [47]. In this paper we only focus in the study of $F = H$ but the formalism could be easily extended to Z and $W^\pm$.

The terms in square brackets in Eq. (42) are encoded in a new Monte Carlo generator `HN3LO` up to the third order in the strong coupling constant. After expanding Eq. (7) to this order, several non-trivial convolutions emerge and we document the corresponding formulae implemented in `HN3LO` in Appendix A. All our results up to the NNLO level are in agreement with the Monte Carlo generator `HNNLO` [1] at the per mille level of accuracy. On the right-hand side of Eq. (36), the partonic Higgs boson total cross sections at NNLO ($\left[\hat{\sigma}^{\text{tot}}_H\right]_{\text{NNLO}}$) and N^{3}LO ($\left[\hat{\sigma}^{\text{tot}}_H\right]_{\text{N}^3\text{LO}}$) are also required. We use the analytical coefficient function for the total Higgs boson cross section at N^{3}LO $\left[\sigma^{\text{tot}}_H\right]_{\text{N}^3\text{LO}}$ (i.e. $\left[\hat{\sigma}^{\text{tot}}_H\right]_{\text{N}^3\text{LO}}$ convoluted with the PDFs) calculated recently in Ref. [13] and employ the numerical code `ihixs 2` [48] to compute not only the N^{3}LO cross section, but also any of the analytical total cross sections ingredients required to extract the missing coefficient C_{N3}.

The numerical computation of the integral of the difference $\mathrm{d}\sigma^{F+\text{jets}}_{\text{NNLO}} - \mathrm{d}\sigma^{F\ \text{CT}}_{\text{N}^3\text{LO}}$ in Eq. (31), although finite, requires the introduction of a suitable technical lower bound or q_T^{cut}, since both terms in this difference are logarithmically divergent at $q_T^{\text{cut}} \to 0$. This technical cut introduces systematic uncertainties to both $\mathrm{d}\sigma^{F+\text{jets}}_{\text{NNLO}}$ and $\mathrm{d}\sigma^{F\ \text{CT}}_{\text{N}^3\text{LO}}$. Once cancellations between the terms on the right-hand side of Eq. (42) take place, the numerically calculated total cross sections and differential distributions have to be q_T^{cut} independent (within the statistical errors) over some range of q_T^{cut}. At the lower end of this range, numerical instabilities in $\mathrm{d}\sigma^{F+\text{jets}}_{\text{NNLO}}$ (arising from the large dynamical range in this calculation) will limit the accuracy of the result, while at the higher end of the range, missing non-logarithmic terms in $\mathrm{d}\sigma^{F\ \text{CT}}_{\text{N}^3\text{LO}}$ will start to become significant. The numerical stability of $\mathrm{d}\sigma^{F+\text{jet}}_{\text{NNLO}}$ at small q_T using `NNLOJET` has been systematically validated for Higgs boson production (with $q_T^{\text{cut}} = 0.7$ GeV in Ref. [34]) and Drell–Yan production (with $q_T^{\text{cut}} = 2$ GeV in Ref. [35]) at the LHC. In Sections 3.2, 4.1, 4.2 and 4.3, we document numerical results obtained with the q_T subtraction formalism using $q_T^{\text{cut}} = (2 \pm 1)$ GeV.

3.2 The numerical extraction of C_{N3}

In the following, we describe the numerical results regarding the extraction of the C_{N3} coefficient and the corresponding N^{3}LO total cross section.

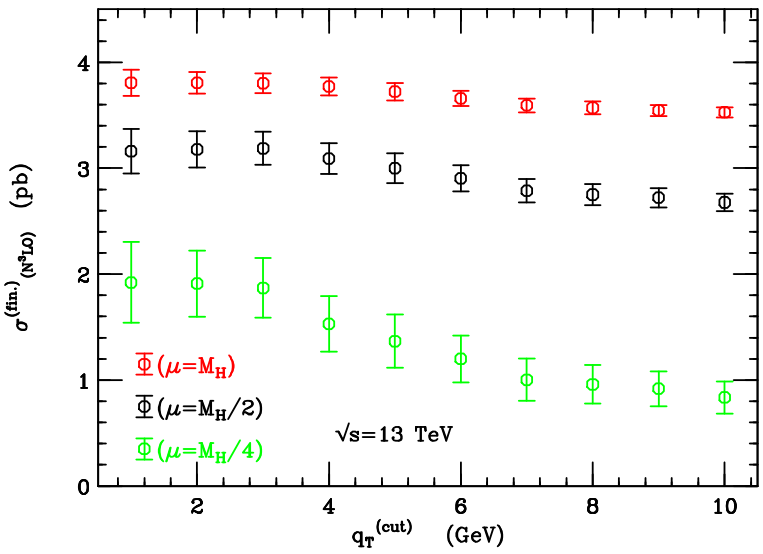

Figure 1: The q_T integrated finite contribution to the cross section of Eq. (31) at N^{3}LO-only (i.e. N^{3}LO-NNLO) between $q_T^{\rm cut}$ and ∞, for three different scales ($\mu = \mu_R = \mu_F$).

In Fig. 1 we display the $\sigma^{(\mathrm{fin.})}_{F=H}$ (i.e. $\hat{\sigma}^{(\mathrm{fin.})}_{H}$ convoluted with the parton distribution functions) cross section at N^{3}LO-only as a function of the $q_T^{\rm cut}$. With N^{3}LO-only we denote $\left[\sigma^{(\mathrm{fin.})}_{H}\right]_{\mathrm{N^3LO}} - \left[\sigma^{(\mathrm{fin.})}_{H}\right]_{\mathrm{NNLO}}$. Using Eq. (35) with Eq. (36) and the value of the resulting integral $\sigma^{(\mathrm{fin.})}_{H}(q_T^{\rm cut} = 1$ GeV) in Fig. 1, it is possible to obtain the q_T integrated cross section of the unknown terms on the right-hand side of Eq. (41) and consequently extract C_{N3}.

The behaviour of the N^{3}LO $\sigma^{(\mathrm{fin.})}_{H}$ cross section as a function of $q_T^{\rm cut}$ in Fig. 1 allows also to estimate the systematical uncertainty corresponding to the use of this technical cut which turns out to be at the *per mille* level in the domain $q_T^{\rm cut} = (2 \pm 1)$ GeV. More specifically, variations of the $q_T^{\rm cut}$ parameter from $q_T^{\rm cut} = 1$ GeV to 3 GeV produce variations in the resulting $\sigma^{(\mathrm{fin.})}_{H}$ cross section of the order of the 0.1%.

In Fig. 2 we show the C_{N3} value obtained for each scale choice ($\mu = M_H/4$, $M_H/2$ and M_H, black points). Notice that the central value of each C_{N3} is independent of the scale (within the uncertainties), in complete agreement with Eq. (35). This scale independence of C_{N3} is unrelated to the used ansatz of Eq. (41): the terms in the right-hand side of Eq. (35) are all scale-independent and the relation between C_{N3} and $\widetilde{H}_g^{H;(3)}$ is defined through Eqs. (35), (40) and (41). The size of the uncertainties shown in Fig. 2 are calculated with the conventional error propagation and are almost entirely due to the size of the statistical uncertainties of the N^{3}LO $\sigma^{(\mathrm{fin.})}_{H}$ cross section in Fig. 1.

The solid red central line in Fig. 2, is the average value calculated from the three different scale choices, whereas the red band is a conservative estimate of the residual uncertainty, which is estimated by considering the coherent average of the statistical uncertainties. The value of the resulting coefficient using the three scales presented in Fig. 2 is $C_{N3} = -932 \pm 224$.

Besides these three central scales we also considered four additional scale choices that complete

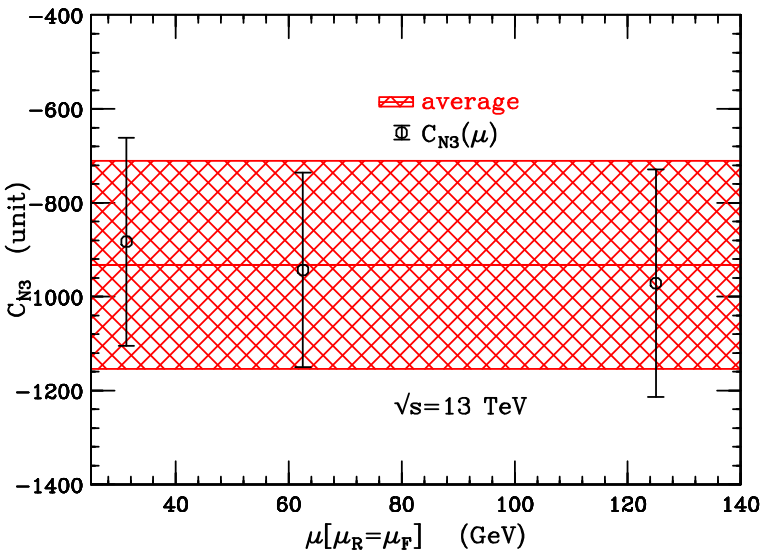

Figure 2: The numerically extracted C_{N3} coefficient as defined in Eq. (41) (black points) for the particular case of $q_T^{\rm cut} = 1$ GeV. The black error bars for each C_{N3} point are obtained propagating the statistical uncertainties of the different terms involved in the computation. The red band is calculated with the average of the three particular C_{N3} values for each scale as detailed in the text.

a seven–point scale variation. Fig. 3 shows the extracted C_{N3} coefficients corresponding to each of the seven scales as a function of the label of the scale as stated in Table 1. The red band and central value (red line) is calculated with the first three black points at $q_T^{\rm cut} = 1$ GeV already present in Fig. 2 and detailed in Table 1 in bold typeface. **NG: do not understand what point you are making here. Either, three scales are independent (and the rest not) in which case you simply confirm that the extra scales are irrelevant. Or, use the seven scale variation from the beginning and drop fig 2. Need to have another pass over this bit.**

Fig. 3 also compares the extracted C_{N3} coefficients for different $q_T^{\rm cut}$ values; $q_T^{\rm cut} = 1$ GeV (black points), $q_T^{\rm cut} = 2$ GeV (blue points) and 3 GeV (green points). The variation of the $q_T^{\rm cut}$ around 2 GeV quantifies the stability of the C_{N3} extraction.

The central value for the C_{N3} coefficient was obtained only using the three central scales $\mu = M_H, M_H/2, M_H/4$ since the other four scales, which are correlated with the previous, do not provide new and independent information to the average. Even more, considering the average over the seven scales, this will result in a shift of -30 units in the central value of C_{N3}, which at the level of the total cross sections (at each scale) represents an effect of less than 0.1%. For the estimation of the uncertainty on C_{N3}, considering the seven scales has no impact. In Sec. 4.2 we will see how the uncertainty associated with the C_{N3} parameter affects the differential distributions.

Whereas the C_{N3} coefficient is independent of the scale choice, its resulting cross section, after convolution with the PDFs (which depend on μ_F) and the strong coupling constant $\alpha_{\rm s}(\mu_R)$, does depend on the scale choice. In Table 1 we collect all values for the C_{N3} coefficients as determined using the different scales and values for $q_T^{\rm cut}$ ($q_T^{\rm cut} = 2 \pm 1$ GeV).

The numerically calculated C_{N3} coefficient allows the total cross section to be computed at

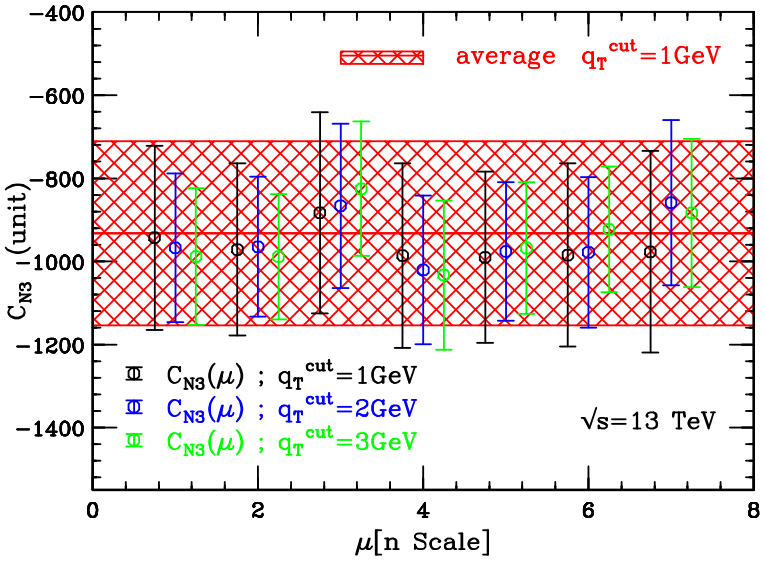

Figure 3: The numerically extracted C_{N3} coefficient (for three different values of $q_T^{\rm cut}$) as a function of the combination of scales, as enumerated in Table 1. The error bars for each particular C_{N3} point are obtained propagating the statistical uncertainties of the different terms involved in the computation. The red band is calculated with the average of the three particular C_{N3} values of the three scales present in Fig. 2 at $q_T^{\rm cut} = 1$ GeV, as detailed in the text.

N^{3}LO using the q_T subtraction method, which serves as a closure test of the approach and the approximations used, and allows the impact of uncertainties associated with the numerical evaluation of the ingredients to be quantified. In Fig. 4 we compare the fully analytical N^{3}LO Higgs boson total cross section [13] (black points) and our best estimation (green points) for three central scales, using $q_T^{\rm cut} = 1$ GeV. The blue squared points represent our best approximation without the use of the C_{N3} coefficient (i.e. $C_{N3} = 0$), that can be considered as the prediction of the q_T subtraction method in the case in which the total cross section is unknown (e.g. for Drell–Yan at N^{3}LO). The uncertainty bars in the q_T subtraction prediction correspond to the statistical errors of the numerical computations and are mainly due to the finite contribution in Eq. (31) at N^{3}LO-only. The magenta and cyan points correspond to our N^{3}LO prediction using $q_T^{\rm cut} = 2$ GeV and 3 GeV respectively. Notice that the $q_T^{\rm cut}$ variation is performed at N^{3}LO-only, while the NNLO cross section is evaluated at fixed $q_T^{\rm cut}$ parameter. The NNLO cross section is also shown in Fig. 4 (red star points) in order to put the size of the N^{3}LO corrections in relation to the previous perturbative order. The total cross sections shown in Fig. 4 are reported in Table 2.

4 The rapidity distribution of the Higgs boson

In this section we use the C_{N3} coefficient (extracted in Sec. 3.2) to produce differential predictions at N^{3}LO. In particular, we present differential results for the rapidity distribution of the Higgs boson. In Sec. 4.1 we estimate at NNLO the uncertainties introduced in the rapidity distribution, by the procedure proposed in Eq. (41). In Sec. 4.2 we present the rapidity distribution at N^{3}LO with the corresponding estimation of the uncertainties associated to the variation of the $q_T^{\rm cut}$ and

n	$\left[\tilde{\mu_R}, \tilde{\mu_F}\right] \times M_H$	C_{N3} ($q_T^{\rm cut} = 1$ GeV)	C_{N3} ($q_T^{\rm cut} = 2$ GeV)	C_{N3} ($q_T^{\rm cut} = 3$ GeV)
(1)	$\left[1/2, 1/2\right]$	$\mathbf{-943 \pm 222}$	-967 ± 179	-988 ± 164
(2)	$\left[1, 1\right]$	$\mathbf{-971 \pm 207}$	-965 ± 168	-989 ± 151
(3)	$\left[1/4, 1/4\right]$	$\mathbf{-883 \pm 243}$	-866 ± 198	-850 ± 162
(4)	$\left[1/2, 1\right]$	-986 ± 222	-1021 ± 179	-1033 ± 179
(5)	$\left[1, 1/2\right]$	-990 ± 206	-976 ± 167	-968 ± 158
(6)	$\left[1/2, 1/4\right]$	-985 ± 221	-978 ± 181	-923 ± 152
(7)	$\left[1/4, 1/2\right]$	-977 ± 243	-859 ± 199	-883 ± 179

Table 1: Extracted values of the C_{N3} coefficients as a function of the $q_T^{\rm cut}$ as shown in Fig. 3 for each scale choice. In bold typeface the C_{N3} coefficients (for the case $q_T^{\rm cut}$ =1 GeV) which are used to compute the averaged value $C_{N3} = -932 \pm 224$ shown in Figs. 2 and 3, with the central red line and the corresponding red band. The uncertainty for each one of the C_{N3} coefficients is calculated with the customary propagations of the uncertainties. The first column is used to label each particular scale choice used in Fig. 3.

$\sigma_H^{\rm tot}$ (pb)	Exact	q_T subtraction ($q_T^{\rm cut} = 1$ GeV)	q_T subtraction ($q_T^{\rm cut} = 2$ GeV)	q_T subtraction ($q_T^{\rm cut} = 3$ GeV)	q_T subtraction ($C_{N3} = 0$)
N^{3}LO [$\mu = M_H/2$]	44.97	44.98 ± 0.21	45.00 ± 0.17	45.02 ± 0.15	45.86 ± 0.21
N^{3}LO [$\mu = M_H$]	43.50	43.52 ± 0.12	43.52 ± 0.10	43.53 ± 0.09	44.08 ± 0.12
N^{3}LO [$\mu = M_H/4$]	45.06	44.98 ± 0.38	44.96 ± 0.31	44.93 ± 0.28	46.44 ± 0.38
NNLO [$\mu = M_H/2$]	43.47	43.46 ± 0.02	43.46 ± 0.02	43.46 ± 0.02	43.46 ± 0.02
NNLO [$\mu = M_H$]	39.64	39.62 ± 0.02	39.62 ± 0.02	39.62 ± 0.02	39.62 ± 0.02
NNLO [$\mu = M_H/4$]	47.33	47.33 ± 0.02	47.33 ± 0.02	47.33 ± 0.02	47.33 ± 0.02

Table 2: The total cross section for Higgs boson production $\sigma_H^{\rm tot}$ at the LHC ($\sqrt{s} = 13$ TeV). Results for NNLO and N^{3}LO cross sections for three different scales $\mu = M_H/2$ (central scale), $\mu = M_H$ and $\mu = M_H/4$. The column ''Exact'' contains the results of Ref. [13] computed with the numerical code of Ref. [48] as detailed in the text. The results with the q_T subtraction method are obtained using three different values of $q_T^{\rm cut}$ (1,2 and 3 GeV), and their uncertainties are calculated with the customary propagation of statistical errors. The last column shows $\sigma_H^{\rm tot}$ obtained with the q_T subtraction method and using $C_{N3} = 0$ at N^3LO. The values of $\sigma_H^{\rm tot}$ reported in this Table are shown in Fig. 4. The NNLO cross sections computed with the q_T subtraction method are obtained using $q_T^{\rm cut} = 1$ GeV, i.e. the variation of this parameter in the N^{3}LO cross section is considered at N^{3}LO-only.

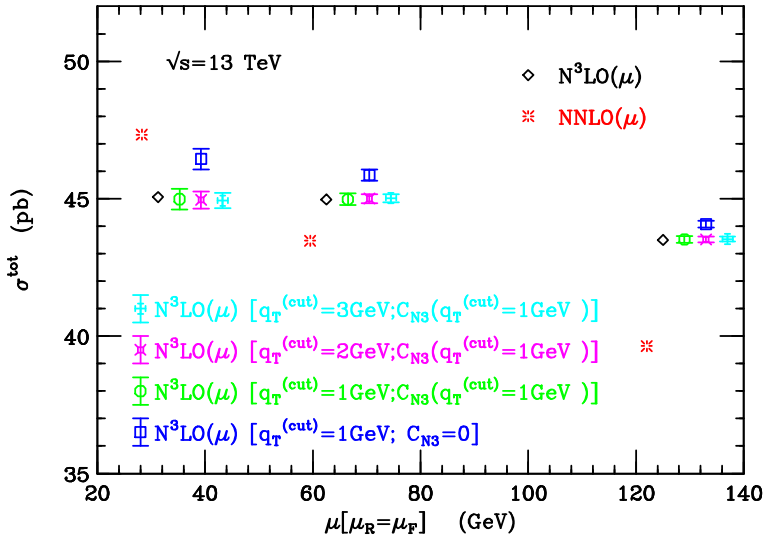

Figure 4: Total cross section of Higgs boson production, $\left[\sigma_H^{\rm tot}\right]_{\rm N^3LO}$, as obtained by the q_T subtraction formalism, compared with the corresponding analytical $\left[\sigma_H^{\rm tot}\right]_{\rm N^3LO}$ of Ref. [13] (black diamonds). Green points denote the q_T subtraction prediction for $q_T^{\rm cut}$=1 GeV, magenta points are $\left[\sigma_H^{\rm tot}\right]_{\rm N^3LO}$ using $q_T^{\rm cut}$=2 GeV, and cyan using $q_T^{\rm cut}$=3 GeV. Whereas the $q_T^{\rm cut}$ is changed (from 1 to 3 GeV) the coefficient C_{N3} is always considered the same (as extracted in Fig. 2 for $q_T^{\rm cut}$=1 GeV). The q_T subtraction prediction at N^{3}LO with the C_{N3} numerical coefficient fixed to zero (using $q_T^{\rm cut}$=1 GeV) is shown with blue squared points. The NNLO analytical Higgs boson cross section ($\left[\sigma_H^{\rm tot}\right]_{\rm NNLO}$) is represented by red points. All the cross sections are shown for three different scales: $\mu \equiv \mu_R = \mu_F = \{1/4, 1/2, 1\} M_H$ and horizontally displaced for better visibility. The uncertainty bars in the q_T subtraction predictions are calculated with the customary propagation of statistical uncertainties.

C_{N3} parameters.

4.1 The NNLO rapidity distribution

In this section we aim to quantify the uncertainty in the approximation used in Eq. (41). This approximation was first proposed in Ref. [2] for Higgs production at NNLO. Since all the ingredients of the q_T subtraction formalism at NNLO are now known in analytical form [25], it is possible to evaluate the deviation caused by the approximation from the exact result. This analysis allows to assess the deviation from the exact result that could be present at N^{3}LO in Sec. 4.2 and 4.3 below. For this quantitative study we consider the collinear functions $C_{g\,a}^{(1)}$ and the hard–virtual factor $H_g^{H;(1)}$ in Eq. (34) as known. The collinear functions $C_{g\,a}^{(2)}$ and the first order helicity-flip functions $G_{g\,a}^{(1)}$ are regarded as unknown. The hard–virtual factor $H_g^{H;(2)}$ is divided in two contributions as in Eq. (40)

$$\widetilde{H}_g^{H;(2)} \equiv H_g^{H;(2)} - \left[H_g^{H;(2)}\right]_{(\delta_{(1)}^{q_T})} , \tag{43}$$

where $\left[H_g^{H;(2)}\right]_{(\delta_{(1)}^{q_T})}$ is considered as unknown for the present NNLO study. These so-called *un-*

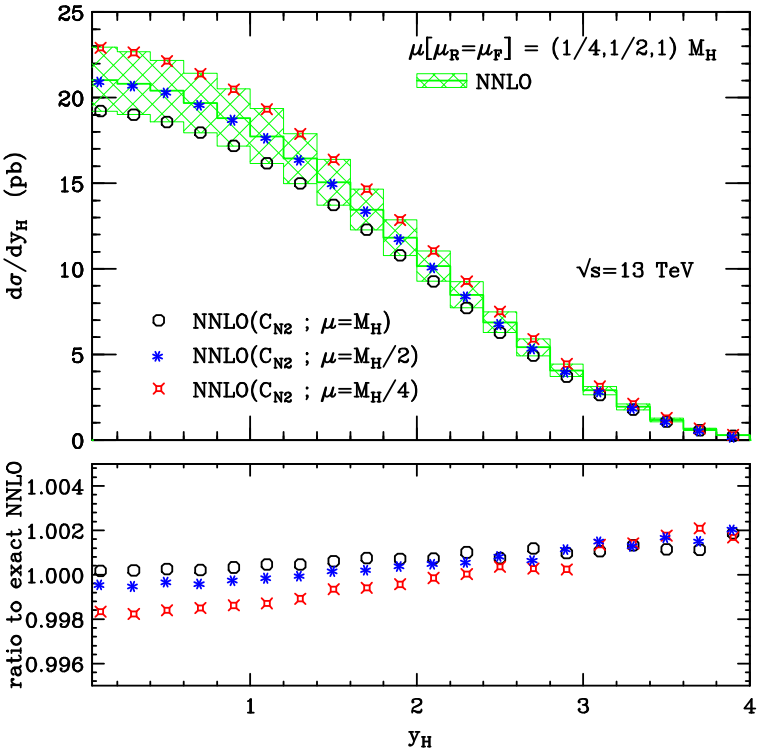

Figure 5: Rapidity distribution at NNLO computed using the q_T subtraction formalism (solid green band) compared with the evaluation using the C_{N2} numerical coefficient (red, blue and black points). In the lower panel we show the ratio to the exact NNLO result. For this particular example at NNLO, we employ the three-point scale variation: $\mu = \mu_R = \mu_F = \{M_H/4, M_H/2, M_H\}$.

known functions (for this exercise) which depend on the variable z in Eq. (34) are approximated with a single numerical coefficient C_{N2} proportional to $\delta(1-z)$ (the C_{N2} here was labeled as C_N in Ref. [2]):

$$C_{N2}\;\; \delta_{g\,a}\,\delta_{g\,b}\,\delta(1-z) \;\;\leftarrow\;\; \delta_{g\,a}\,\delta_{g\,b}\,\delta(1-z)\,\left[H_g^{H;(2)}\right]_{(\delta_{(1)}^{qT})} + \delta_{g\,a}\,C_{g\,b}^{(2)}(z) + \delta_{g\,b}\,C_{g\,a}^{(2)}(z) + \left(G_{g\,a}^{(1)} \otimes G_{g\,b}^{(1)}\right)(z) \;\; . \tag{44}$$

In Fig. 5 we show the rapidity distribution of the Higgs boson at NNLO computed with the exact q_T subtraction (green band) and the NNLO prediction using the C_{N2} coefficient (red, blue and black points). For this particular example at NNLO, we employ the three–point scale variation: $\mu = \mu_R = \mu_F = \{M_H/4, M_H/2, M_H\}$. Repeating the analysis performed for the completion of Table 1, and Fig. 2 we arrive to the following result: $C_{N2} = 28 \pm 1$. The numerical value of the C_{N2} parameter corresponds to a specific $\widetilde{H}_g^{H;(2)}$ hard coefficient:

$$\widetilde{H}_g^{H;(2)} = \frac{11399}{144} + \frac{19}{8}L_t - \frac{1189}{144}N_f + \frac{2}{3}N_f L_t + \frac{83}{6}\pi^2 - \frac{5}{18}\pi^2 N_f + \frac{13}{16}\pi^4 - \frac{165}{4}\zeta_3 + \frac{5}{6}N_f\zeta_3 \;\; , \tag{45}$$

which is obtained with the same method that was used to arrive to Eq. (39). Using this C_{N2} parameter we can produce differential predictions which are obtained *mimicking* the strategy that we intend to use at N^{3}LO.

In the lower panel of Fig. 5 we show the ratio to the exact NNLO result, i.e. we present the ratio for each scale. As expected, the approximation presents its best behaviour at central rapidity

and the deviation from the exact results is at *per mille* level throughout the presented rapidity region of $|y_H| \leq 4$.

The numerical implementation of the q_T subtraction method (more precisely Eq. (38) at NNLO) requires the use of a lower technical cut ($q_T^{\rm cut}$) in the integral performed over the transverse momentum of the finite contribution in Eq. (31). The computation of the NNLO Higgs boson cross section and differential distributions do not constitute a big numerical challenge, and the $q_T^{\rm cut}$ can be chosen as low as the computation demands. We performed variations of the $q_T^{\rm cut}$ value between 0.1 GeV and 3 GeV, and the NNLO cross sections (and differential distributions) present deviations within an interval of 0.5% level (the largest deviation 0.5% is always observed for the scale choice $\mu = M_H/4$).

4.2 Numerical stability of the N^{3}LO rapidity distribution

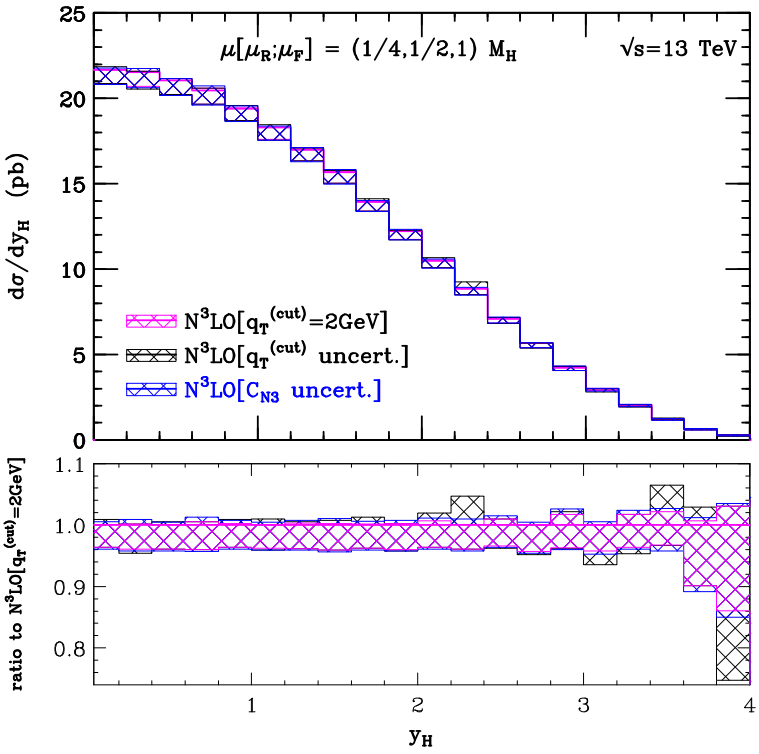

Figure 6: Rapidity distribution of the Higgs boson as computed using the q_T subtraction formalism at N^{3}LO. All bands include the seven-point scale variation as detailed in Table 2. The magenta band constitutes our result with $q_T^{\rm cut} = 2$ GeV using the central value for the C_{N3} coefficient ($C_{N3} = -932$). The black band is obtained as the envelope between the prediction at $q_T^{\rm cut} = 1$ GeV and 2 GeV using $C_{N3} = -932$. The blue band is computed at fixed $q_T^{\rm cut} = 2$ GeV taking the two extremal values of the C_{N3} coefficient according to the calculated uncertainty ($C_{N3} = -932 \pm 224$), and performing seven-point scale variation, as described in the text.

In this section, we quantify the numerical stability (as well as the involved intrinsic uncertainties) of the Higgs boson rapidity distributions at N^{3}LO regarding the $q_T^{\rm cut}$ and C_{N3} parameters and the statistical uncertainties introduced by $\mathrm{d}\sigma_{F=H}^{(\rm fin.)}/\mathrm{d}y_H$ at N^{3}LO-only.

In Fig. 6 we show the rapidity distribution at N^{3}LO obtained with the q_T subtraction method using the C_{N3} coefficient extracted in Sec. 3.2 ($C_{N3} = -932 \pm 224$). The NNLO prediction is always computed with $q_T^{\rm cut} = 1$ GeV. The magenta band in Fig. 6 is computed using $q_T^{\rm cut} = 2$ GeV and performing the seven-point scale variation specified in Table 2.

The black band is calculated as the envelope of the scale variation bands for two different values of $q_T^{\rm cut}$: 1 GeV and 2 GeV. Therefore, the black band in Fig. 6 can be taken as estimation of the uncertainty due to the implementation of different $q_T^{\rm cut}$ parameters at N^{3}LO exclusively. In Fig. 4 (and Table 2), we observed that the total cross section (for the three central scales) is rather stable as a function of the $q_T^{\rm cut}$. The variations of the N^{3}LO cross sections were at the *per mille* level of accuracy if we consider $q_T^{\rm cut} = 2 \pm 1$ GeV, which is far better than the associated statistical uncertainty (see Table 2). The estimation of the uncertainty due to the $q_T^{\rm cut}$ variation performed in Fig. 6, differential in the rapidity of the Higgs boson, confirms the stability of the total cross section reported in Table 2. The rapidity distribution is almost insensitive to the change in the $q_T^{\rm cut}$ parameter in the region where the bulk of the cross section is concentrated ($|y_H| \leq 3.6$). At large rapidities ($|y_H| \sim 4$), where the overall contribution to the total cross section is less than 0.5%, we found the largest deviations. Such deviations are mainly related to the numerical uncertainties from $\mathrm{d}\sigma^{(\rm fin.)}_{F=H}/\mathrm{d}y_H$ at N^{3}LO-only.

Finally, we consider the uncertainty introduced by the statistical errors of the C_{N3} coefficient. The blue band in Fig. 6 is obtained as the envelope of the seven-point scale variation at $q_T^{\rm cut} =$ 2 GeV now considering for each scale the two extremal C_{N3} coefficients corresponding to its maximum and minimum statistical deviations: $C_{N3} = \{-1156, -708\}$. Therefore the envelope is taken from a total of 14 rapidity distributions (two extremal predictions for each one of the seven scales). The net effect of this C_{N3} variation result in an overall enlargement of the magenta band at $q_T^{\rm cut} = 2$ GeV. Our final estimation of the uncertainties in the rapidity of the Higgs boson at N^{3}LO is computed as the envelope of three bands: seven-point scale variation only, combined with $q_T^{\rm cut}$ variation, combined with C_{N3} variation.

4.3 The rapidity distribution of the Higgs boson at N^{3}LO

In this section we present our predictions for the Higgs boson rapidity distributions at the LHC, applying the N^{3}LO q_T subtraction method presented in Sec. 2. The setup of the calculation was described in Sec. 3.2. Fig. 7 shows the rapidity distribution of the Higgs boson at LO (dashed black band), NLO (blue solid band), NNLO (green solid band) and N^{3}LO (magenta solid band). The N^{3}LO band is computed taking into account the uncertainties due to $q_T^{\rm cut}$ and C_{N3} as explained in Sec. 4.2. **AH: Nicer to separate scale uncertainties from the rest? Maybe show bands = scale and error bars for the $q_T^{\rm cut}$ etc. uncert.?**

The central scale ($\mu = M_H/2$) is shown with a solid line while the variation of the scales by a factor $\{1/2, 2\}$ is producing the seven-point scale variation band. It is interesting to notice that from LO to NNLO, the scale $\mu = M_H/2$ is always at the center of the corresponding scale variation band in Fig. 7. At N^{3}LO the central scale $\mu = M_H/2$ (magenta solid line) almost coincides with the upper edge of the band, as was already observed for the total cross section [12, 13], see Table 2 and Fig. 4. Figures 4 and 7 show a substantial reduction in the size of the scale variation band at N^{3}LO, in the total cross section and in differential distributions, respectively.

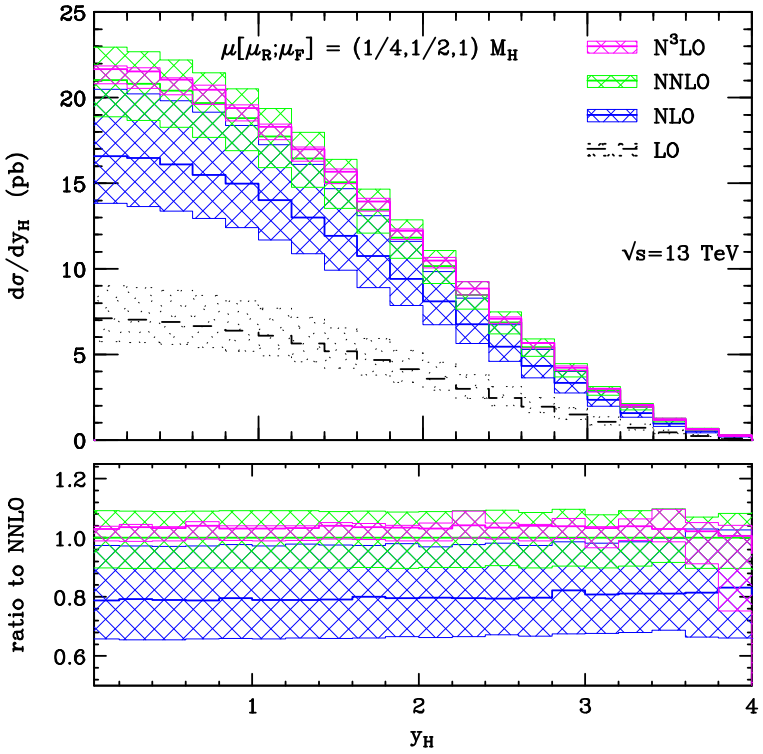

Figure 7: Rapidity distribution of the Higgs boson computed using the q_T subtraction formalism up to N^{3}LO. The seven-point scale variation bands (as stated in Table 1) of the LO, NLO, NNLO and N^{3}LO(C_{N3}) results are as follows: LO (black dashed), NLO (blue solid), NNLO (green solid) and N^{3}LO(C_{N3}) (magenta solid). The central scale ($\mu = M_H/2$) at each perturbative order is shown with solid lines. In the lower panel, the ratio to the NNLO prediction is shown. While the bands for the predictions at LO, NLO and NNLO are computed with the seven scales as detailed in the text, the N^{3}LO(C_{N3}) band is obtained after considering also the uncertainties due to the variation of the $q_T^{\rm cut}$ and the C_{N3} coefficient in the N^{3}LO-only contribution.

In the central rapidity region of $|y_H| \leq 3.6$, the impact of the N^{3}LO corrections on the NNLO result is almost independent of y_H with a flat K-factor about 1.035 for the central scale choice. The combined theoretical uncertainty at N^{3}LO is at most of $\pm 5\%$ level with respect to the central scale choice. The uncertainty on the y_H distribution is reduced by more than 50% from NNLO to N^{3}LO. The N^{3}LO theoretical uncertainty band stays within the scale variation band of NNLO except for the very large rapidity region.

The N^{3}LO corrections to the Higgs boson rapidity distribution have been investigated recently in [15], where an analytic calculation of the leading terms of the threshold expansion of the rapidity-differential coefficient function was presented. Based on the behaviour of the threshold expansion for the total cross section [12], it is anticipated that the currently known terms in the threshold expansion for the rapidity distribution [15] are not yet sufficient to provide a proper description. Comparing Fig. 7 with the results obtained in Ref. [15], although with different choices of PDFs and scale variation prescriptions, we observe that the central scale N^{3}LO values for the rapidity region $y_H < 0.5$ agree well between the two calculations. Both calculations demonstrate a considerable reduction of the scale variation band from NNLO to N^{3}LO in this central rapidity region. For the rapidity region $y_H > 1$, substantial differences between the two

calculations appear, with q_T subtraction generally yielding considerably smaller N^{3}LO corrections (within the NNLO scale uncertainty band) than what is observed from the leading terms in the threshold expansion.

5 Conclusions and outlook

In this paper we have performed a detailed study of Higgs boson production at the LHC using the q_T subtraction formalism at N^{3}LO. We systematically describe the q_T subtraction formalism using the hard resummation scheme for a generic colourless and massive system $F(\{q_i\})$ produced at hadron colliders. Fully differential cross sections for this type of final state system are separated into $\delta(q_T)$ and $q_T \neq 0$ contributions. The contribution for $q_T \neq 0$ is calculated, using a phase space cut-off $q_T^{\rm cut}$, as the difference between $F(\{q_i\})$+jets production and q_T counter-terms. Specifically, we use the `NNLOJET` package to compute NNLO Higgs-plus-jet production and expand the Sudakov from factor in the hard resummation scheme to the matching order for the corresponding q_T counter-terms. The contribution at $\delta(q_T)$ is further factorized into convolutions of the Sudakov form factor, the hard–virtual function, the helicity-flip coefficient function, the hard–collinear coefficient function as well as the parton distribution functions (Sec. 2). The factorization under the hard resummation scheme guarantees that all the process-dependent contributions proportional to a form factor are included in the hard–virtual function which depends on both initial- and final-state particles. All other factorized contributions only depend on the initial states. Some of the factorized ingredients contributing at $\delta(q_T)$ are not known analytically at N^{3}LO for the moment. We collect all analytically available contributions and approximate the unknown pieces by a constant coefficient C_{N3} which is scale- and process-independent (Sec. 3). Using the available inclusive total cross section for N^{3}LO Higgs production and the known pieces from the q_T subtraction formalism, we numerically extract the value of C_{N3}. By comparing the numerical values for C_{N3} using different scales and $q_T^{\rm cut}$ setups in the extraction, we conclude from mutually consistent results that C_{N3} is independent of the scale choice with the averaged value of $C_{N3} = -932 \pm 224$ (Sec. 3.2).

As a proof-of-concept implementation of the q_T subtraction method at N^{3}LO, we calculate the total cross section and rapidity distributions for Higgs boson production at LHC using a new Monte Carlo generator `HN3LO`. Using the same averaged value of C_{N3}, we produce the inclusive total cross section in three different scale choices and find excellent agreement with the exact results (from `ihixs 2` [48]) at 0.02% level of accuracy for all three scales. For the differential rapidity distribution of the Higgs boson, we first study the systematic error from the C_{N3} approximation by considering the NNLO calculation and introducing an approximate C_{N2}. The NNLO y_H distribution exhibit per mille level agreement between the C_{N2} approximation and the exact result, supporting the reliability of the procedure. We calculate the y_H distribution at N^{3}LO employing a seven-point scale variation and carefully assess systematic errors arising form different $q_T^{\rm cut}$ and C_{N3} values. Compared to the NNLO y_H distributions, we observe a large reduction of theory uncertainties by more than 50% at N^{3}LO. The scale variation band at N^{3}LO stays within the NNLO band with a flat K-factor of about 1.035 in the central rapidity region ($|y_H| \leq 3.6$). Both the systematic error analysis and the phenomenological predictions confirm that our calculations at N^{3}LO using q_T subtraction formalism are well under control. The approximation related to the C_{N3} coefficient in our approach can be easily replaced by the full analytical results once available.

With the upcoming larger data set and more accurate measurements of Higgs properties at the phenomenologialLHC, we prepare precise theoretical tools that could match the frontier accuracy of experimental results. More differential properties at N^{3}LO involving the Higgs boson and its decay products can be studied using the same framework established in this paper. The current N^{3}LO calculation, using the approximation of large top quark mass, attains a level of precision that several other contributions will need to taken into account for a full study of precision phenomenology [49]: finite top quark mass effects, heavy-light quark interference contributions and electroweak corrections.

Acknowledgements

LC would like to thank Stefano Catani for very useful and valuable discussions. XC would like to thank Javier Mazzitelli and Hua Xing Zhu for inspiring discussions. We thank the University of Zurich S3IT and CSCS Lugano for providing the computational resources for this project. This research was supported in part by the UK Science and Technology Facilities Council, by the Swiss National Science Foundation (SNF) under contracts 200020-175595 and CRSII2-160814, by the Swiss National Supercomputing Centre (CSCS) under project ID UZH10, by the Research Executive Agency (REA) of the European Union under the ERC Advanced Grant MC@NNLO (340983).

Appendix

A Convolutions at N^{3}LO

The numerical implementation of Eq. (7) requires the computation of several convolutions between splitting functions, collinear and helicity-flip functions. In principle, taking the N-moments of the functions involved in the calculation, one can avoid the use of convolutions, since in N-space they correspond to simple products. However, the numerical implementation of Eq. (7) in the Monte Carlo code `HN3LO` was carried out in the z-space (e.g. as in the codes `HNNLO` [1], `DYNNLO` [50], `2γNNLO` [51], etc.), and therefore the new third order convolutions have to be calculated as well.

The convolutions in Eqs. (34), (35), (41) and (44) between two functions ($f(z)$ and $g(z)$) of the the variable z are defined through the following integral

$$(f \otimes g)(z) \equiv \int_z^1 \frac{\mathrm{d}y}{y}\, f\left(\frac{z}{y}\right)\, g(y)\,. \tag{46}$$

In the case of processes initiated by gluon fusion, the complete list of third order convolutions to be calculated can be found in Table 3. All the remaining convolutions in Eq. (7) at N^{3}LO already contributed to the previous orders and they are regarded as known. The symbol $\gamma_{ab}^{(n)}$ in Table 3 denotes the usual splitting functions of nth-order and they contribute to Eq. (7)) since the PDFs have to be evolved from the scale b_0^2/b^2 to the factorization scale μ_F. The first three rows in Eq. (3) were calculated in Ref. [53] and cross-checked with a dedicated computation for the results presented in this paper. The public `Mathematica` package `MT` [52] is used to calculate the necessary convolutions (i)–(vi) in Ref. [53], which can be further expressed in terms of *harmonic*

(i)	$\gamma_{ga}^{(1)} \otimes \gamma_{ab}^{(1)} \otimes \gamma_{bg}^{(1)}$	(ii)	$\gamma_{ga}^{(1)} \otimes \gamma_{ab}^{(1)} \otimes \gamma_{bq}^{(1)}$
(iii)	$\gamma_{ga}^{(1)} \otimes \gamma_{ag}^{(2)}$	(iv)	$\gamma_{ga}^{(1)} \otimes \gamma_{aq}^{(2)}$
(v)	$\gamma_{ga}^{(2)} \otimes \gamma_{ag}^{(1)}$	(vi)	$\gamma_{ga}^{(2)} \otimes \gamma_{aq}^{(1)}$
(vii)	$C_{ga}^{(1)} \otimes \gamma_{ag}^{(2)}$	(viii)	$C_{ga}^{(1)} \otimes \gamma_{aq}^{(2)}$
(ix)	$C_{ga}^{(2)} \otimes \gamma_{ag}^{(1)}$	(x)	$C_{ga}^{(2)} \otimes \gamma_{aq}^{(1)}$
(xi)	$G_{ga}^{(1)} \otimes \gamma_{ag}^{(1)}$	(xii)	$G_{ga}^{(1)} \otimes \gamma_{aq}^{(1)}$

Table 3: Convolutions appearing at the N^{3}LO-only between the collinear $C_{ab}^{(n)}$, the helicity-flip $G_{ab}^{(n)}$ and the splitting functions $\gamma_{ab}^{(n)}$ $(n = 1, 2)$. The repeated subindices a, a and b imply a sum over the parton flavors $q, \bar{q}, g$. The first and last subindices denote the partonic channel in which they are contributing, i.e. the convolutions in the first column are used in the gg partonic channel whereas the second (and last) column is for the qg and gq partonic channels.

polylogarithms (HPLs) [56] using the `Mathematica` package `HPL` [55]. The remaining convolutions in Eqs. (vii)–(xii) of Table 3 were computed for this work. The `MT` [52] package is not able to solve all the convolutions of weight 3 and 4 that are needed in (vii)–(xii). For instance, the `MT` package cannot handle convolutions in which their result has to be expressed in terms of multiple polylogarithms (or *Goncharov polylogarithms* GPLs) [57, 54, 58] as it is the case when the collinear functions $C_{gj}^{(2)}$ are involved. For those, we have computed the convolutions (vii)–(xii) with a newly developed code `Convo`, which is able to provide results in terms of GPLs and also can handle terms that are individually divergent, but finite after addition.

The multiple polylogarithms can be defined recursively, for $n \geq 0$, via the iterated integral [57, 54, 58]

$$G(a_1, \ldots, a_n; z) = \int_0^z \frac{\mathrm{d}t}{t - a_1} G(a_2, \ldots, a_n; t)\,, \tag{47}$$

with $G(z) = G(;z) = 1$ (an exception being when $z = 0$ in which case we put $G(0) = 0$) and with $a_i \in \mathbb{C}$ are chosen constants and z is a complex variable. For the convolutions in Table 3 the variable z and the weights $a_1, \ldots, a_n$ are all real constants.

From the convolutions in Table 3 we quote some examples which appear as building blocks in the computation of Eqs. (vii)–(xii),

$$\left\{ \mathrm{D}_0[1-y]; \frac{1}{y}; 1; y; y^2 \right\} \otimes \left(\frac{f(y)}{1+y} \right) \quad , \tag{48}$$

with

$$f(y) = \left\{ \mathrm{Li}_3\left(\frac{1}{1+y}\right); \mathrm{Li}_3(\pm y); \mathrm{Li}_2(\pm y); \mathrm{Li}_2(1-y); \mathrm{Li}_2(\pm y)\ln(y); \right. \\ \left. \ln^2(1+y)\ln(y); \ln(1+y)\ln^2(y) \right\} \quad , \tag{49}$$

(a)	$G(\frac{z}{1+z},0,0,1;\frac{1}{2})$	(b)	$G(1,0,0,-z;z)$	(c)	$G(0,1,0,-1;z)$
(d)	$G(0,1,0,z;1)$	(e)	$G(0,1,z,0;1)$	(f)	$G(0,z,1,0;1)$
(g)	$G(-z,0,z,0;1)$	(h)	$G(0,1,0,-z;z)$	(i)	$G(0,1,-z,-z;z)$
(j)	$G(-z,1,0,0;1)$	(k)	$G(-z,1,0,0;z)$	(l)	$G(-z,0,0,z;1)$

Table 4: Basis for the GPLs used in the numerical implementation of the convolutions listed in Table 3.

where the *plus* distribution $\mathrm{D}_0[1-z]$ is defined as usual

$$\int_0^1 \mathrm{d}z\; f(z)\; \mathrm{D}_0[1-z] = \int_0^1 \mathrm{d}z\; \frac{f(z)}{(1-z)_+} = \int_0^1 \frac{\mathrm{d}z}{1-z}\,(f(z)-f(1)) \quad . \tag{50}$$

After performing all the convolutions listed in Table 3, their final expressions (each one of the convolutions) are finite in the domain $z \in (0,1)$. Even more, convolutions evaluated in the domain $z \in (0,1)$ produce results in $\mathbb{R}$. It is possible to write the expressions in Table 3 (after simplifying) in terms of twelve GPLs that are not reducible to polylogarithmic functions of type $\mathrm{Li}_n(z)$, and cannot be combined (e.g. through the *shuffle* algebra) with other GPLs in order to produce simpler results. The list of the irreducible GPLs is presented in Table 4. All remaining GPLs appearing in the convolutions of Table 3 can be related to the set given in Table 4 using the results of Refs. [60, 55, 59] and performing the customary *shuffle* algebra. The numerical implementation of the GPLs in Table 4 was made using the package `GiNaC` [61, 62]. The basis of GPLs in Table 4 is not unique, but sufficient for numerical evaluation.

An example of a third order convolution is the following integral

$$\begin{aligned}
&\left(\frac{\mathrm{Li}_3(y)}{1+y} \otimes \mathrm{D}_0[1-y]\right)(z) = \int_z^1 \frac{\mathrm{d}y}{y+z}\;\mathrm{Li}_3\left(\frac{z}{y}\right)\;\frac{1}{(1-y)_+} = \frac{1}{1+z}\Bigg(-\zeta_3 G(0;z) + \frac{i\pi^3}{6}G(0;z) \\
&+\frac{\pi^2}{3}G(-z;1)G(0;z) - i\pi G(-z,0;1)G(0;z) - G(-z,0,0;1)G(0;z) + \frac{i\pi\zeta_3}{4} + \frac{\pi^2}{3}G(0,1;z) \\
&+i\pi G(-z;1)G(0,0;z) - \frac{\pi^2}{6}G(0,0;z) - G(-z;1)G(0,0,0;z) + i\pi G(0,0,1;z) \\
&+G(0,0;z)G(-z,0;1) - \frac{\pi^2}{3}G(-z,0;1) + i\pi G(-z,0,0;1) - G(0,0,0,1;z) \\
&-G(0,0,1,z;1) - G(0,0,z,1;1) - G(0,1,0,z;1) - G(1,0,0,z;z) + G(-z,0,0,0;1) \\
&-G(-z,0,0,z;1) + G(-z,0,0,z;z) + \frac{19\pi^4}{720}\Bigg) \quad .
\end{aligned} \tag{51}$$

References

[1] S. Catani and M. Grazzini, Phys. Rev. Lett. **98** (2007) 222002 [hep-ph/0703012].

[2] G. Bozzi, S. Catani, D. de Florian and M. Grazzini, Nucl. Phys. B **737** (2006) 73 [hep-ph/0508068].

[3] G. Bozzi, S. Catani, D. de Florian and M. Grazzini, Phys. Lett. B **564** (2003) 65. [hep-ph/0302104].

[4] R. Boughezal, X. Liu and F. Petriello, Phys. Rev. D **91** (2015) 094035 [arXiv:1504.02540].

[5] J. Gaunt, M. Stahlhofen, F. J. Tackmann and J. R. Walsh, JHEP **1509** (2015) 058 [arXiv:1505.04794].

[6] M. Czakon, Nucl. Phys. B **849** (2011) 250 [arXiv:1101.0642].

[7] R. Boughezal, K. Melnikov and F. Petriello, Phys. Rev. D **85** (2012) 034025 [arXiv:1111.7041].

[8] M. Cacciari, F. A. Dreyer, A. Karlberg, G. P. Salam and G. Zanderighi, Phys. Rev. Lett. **115** (2015) 082002 Erratum: [Phys. Rev. Lett. **120** (2018) 139901] [arXiv:1506.02660].

[9] A. Gehrmann-De Ridder, T. Gehrmann and E. W. N. Glover, JHEP **0509** (2005) 056 [hep-ph/0505111]; A. Gehrmann-De Ridder, T. Gehrmann and E. W. N. Glover, Phys. Lett. B **612** (2005) 49 [hep-ph/0502110]; A. Gehrmann-De Ridder, T. Gehrmann and E. W. N. Glover, Phys. Lett. B **612** (2005) 36 [hep-ph/0501291]; A. Daleo, T. Gehrmann and D. Maitre, JHEP **0704** (2007) 016 [hep-ph/0612257]; A. Daleo, A. Gehrmann-De Ridder, T. Gehrmann and G. Luisoni, JHEP **1001** (2010) 118 [arXiv:0912.0374]; R. Boughezal, A. Gehrmann-De Ridder and M. Ritzmann, JHEP **1102** (2011) 098 [arXiv:1011.6631]; T. Gehrmann and P. F. Monni, JHEP **1112** (2011) 049 [arXiv:1107.4037]; A. Gehrmann-De Ridder, T. Gehrmann and M. Ritzmann, JHEP **1210** (2012) 047 [arXiv:1207.5779]; J. Currie, E. W. N. Glover and S. Wells, JHEP **1304** (2013) 066 [arXiv:1301.4693].

[10] K. G. Chetyrkin, J. H. Kuhn and A. Kwiatkowski, Phys. Rept. **277** (1996) 189 [hep-ph/9503396].

[11] J. A. M. Vermaseren, A. Vogt and S. Moch, Nucl. Phys. B **724** (2005) 3 [hep-ph/0504242].

[12] C. Anastasiou, C. Duhr, F. Dulat, F. Herzog and B. Mistlberger, Phys. Rev. Lett. **114** (2015) 212001 [arXiv:1503.06056].

[13] B. Mistlberger, JHEP **1805** (2018) 028 [arXiv:1802.00833].

[14] F. A. Dreyer and A. Karlberg, Phys. Rev. Lett. **117** (2016) 072001 [arXiv:1606.00840].

[15] F. Dulat, B. Mistlberger and A. Pelloni, JHEP **1801** (2018) 145 [arXiv:1710.03016].

[16] J. Currie, T. Gehrmann, E. W. N. Glover, A. Huss, J. Niehues and A. Vogt, JHEP **1805** (2018) 209 [arXiv:1803.09973].

[17] Y. L. Dokshitzer, D. Diakonov and S. I. Troian, Phys. Lett. B **79** (1978) 269, Phys. Rep. **58** (1980) 269; G. Parisi and R. Petronzio, Nucl. Phys. B **154** (1979) 427. G. Curci, M. Greco and Y. Srivastava, Nucl. Phys. B **159** (1979) 451; J. C. Collins and D. E. Soper, Nucl. Phys. B **193** (1981) 381 [Erratum-ibid. B **213** (1983) 545], Nucl. Phys. B **197** (1982) 446; J. Kodaira and L. Trentadue, Phys. Lett. B **112** (1982) 66, report SLAC-PUB-2934 (1982), Phys. Lett. B **123** (1983) 335; J. C. Collins, D. E. Soper and G. Sterman, Nucl. Phys. B **250** (1985) 199; S. Catani, E. D'Emilio and L. Trentadue, Phys. Lett. B **211** (1988) 335; D. de Florian and M. Grazzini, Phys. Rev. Lett. **85** (2000) 4678 [hep-ph/0008152];

S. Catani, D. de Florian and M. Grazzini, Nucl. Phys. B **596** (2001) 299 [hep-ph/0008184].

[18] W. Bizon, P. F. Monni, E. Re, L. Rottoli and P. Torrielli, JHEP **1802** (2018) 108 [arXiv:1705.09127].

[19] S. Catani and M. Grazzini, Nucl. Phys. B **845** (2011) 297 [arXiv:1011.3918].

[20] S. Catani, L. Cieri, D. de Florian, G. Ferrera and M. Grazzini, Nucl. Phys. B **881** (2014) 414 [arXiv:1311.1654].

[21] S. Catani, D. de Florian and M. Grazzini, Nucl. Phys. B **596** (2001) 299 [hep-ph/0008184].

[22] O. V. Tarasov, A. A. Vladimirov and A. Y. Zharkov, Phys. Lett. **93B** (1980) 429.

[23] S. A. Larin and J. A. M. Vermaseren, Phys. Lett. B **303** (1993) 334 [hep-ph/9302208].

[24] D. de Florian and M. Grazzini, Nucl. Phys. B **616** (2001) 247 [hep-ph/0108273].

[25] S. Catani and M. Grazzini, Eur. Phys. J. C **72** (2012) 2013 [Erratum-ibid. C **72** (2012) 2132] [arXiv:1106.4652].

[26] S. Catani, L. Cieri, D. de Florian, G. Ferrera and M. Grazzini, Eur. Phys. J. C **72** (2012) 2195 [arXiv:1209.0158].

[27] G. Curci, W. Furmanski and R. Petronzio, Nucl. Phys. B **175** (1980) 27.

[28] W. Furmanski and R. Petronzio, Phys. Lett. B **97** (1980) 437.

[29] R. V. Harlander and K. J. Ozeren, Phys. Lett. B **679** (2009) 467 [arXiv:0907.2997];

[30] S. Catani, Phys. Lett. B **427** (1998) 161 [hep-ph/9802439].

[31] S. Catani, E. D'Emilio and L. Trentadue, Phys. Lett. B **211** (1988) 335.

[32] R. P. Kauffman, Phys. Rev. D **45** (1992) 1512.

[33] D. de Florian and M. Grazzini, Phys. Rev. Lett. **85** (2000) 4678 [hep-ph/0008152].

[34] X. Chen, T. Gehrmann, E.W.N. Glover, A. Huss, Y. Li, D. Neill, M. Schulze, I.W. Stewart, H.X. Zhu, arXiv:1805.00736.

[35] W. Bizon *et al.*, arXiv:1805.05916.

[36] M. Spira, A. Djouadi, D. Graudenz and P. M. Zerwas, Nucl. Phys. B **453** (1995) 17 [hep-ph/9504378].

[37] Y. Li and H. X. Zhu, Phys. Rev. Lett. **118** (2017) 022004 [arXiv:1604.01404].

[38] A. A. Vladimirov, Phys. Rev. Lett. **118** (2017) no.6, 062001 [arXiv:1610.05791].

[39] S. Catani, L. Cieri, D. de Florian, G. Ferrera and M. Grazzini, Nucl. Phys. B **888** (2014) 75 [arXiv:1405.4827].

[40] T. Becher, M. Neubert, Eur. Phys. J. **C71** (2011) 1665 [arXiv:1007.4005].

[41] F. Wilczek, Phys. Rev. Lett. **39** (1977) 1304;
M. A. Shifman, A. I. Vainshtein and V. I. Zakharov, Phys. Lett. B **78** (1978) 443;
T. Inami, T. Kubota and Y. Okada, Z. Phys. C **18** (1983) 69.

[42] R. D. Ball *et al.* [NNPDF Collaboration], JHEP **1504** (2015) 040 [arXiv:1410.8849].

[43] A. Buckley, J. Ferrando, S. Lloyd, K. Nordstrm, B. Page, M. Rfenacht, M. Schnherr and G. Watt, Eur. Phys. J. C **75** (2015) 132 doi:10.1140/epjc/s10052-015-3318-8 [arXiv:1412.7420].

[44] X. Chen, J. Cruz-Martinez, T. Gehrmann, E. W. N. Glover and M. Jaquier, JHEP **1610** (2016) 066 doi:10.1007/JHEP10(2016)066 [arXiv:1607.08817].

[45] A. Gehrmann-De Ridder, T. Gehrmann, E. W. N. Glover, A. Huss and T. A. Morgan, Phys. Rev. Lett. **117** (2016) no.2, 022001 doi:10.1103/PhysRevLett.117.022001 [arXiv:1507.02850].

[46] A. Gehrmann-De Ridder, T. Gehrmann, E. W. N. Glover, A. Huss and T. A. Morgan, JHEP **1611** (2016) 094 doi:10.1007/JHEP11(2016)094 [arXiv:1610.01843].

[47] A. Gehrmann-De Ridder, T. Gehrmann, E. W. N. Glover, A. Huss and D. M. Walker, Phys. Rev. Lett. **120** (2018) no.12, 122001 doi:10.1103/PhysRevLett.120.122001 [arXiv:1712.07543].

[48] F. Dulat, A. Lazopoulos and B. Mistlberger, arXiv:1802.00827.

[49] C. Anastasiou, C. Duhr, F. Dulat, E. Furlan, T. Gehrmann, F. Herzog, A. Lazopoulos and B. Mistlberger, JHEP **1605** (2016) 058 [arXiv:1602.00695].

[50] S. Catani, L. Cieri, G. Ferrera, D. de Florian and M. Grazzini, Phys. Rev. Lett. **103** (2009) 082001 [arXiv:0903.2120].

[51] S. Catani, L. Cieri, D. de Florian, G. Ferrera and M. Grazzini, Phys. Rev. Lett. **108** (2012) 072001 Erratum: [Phys. Rev. Lett. **117** (2016) no.8, 089901] [arXiv:1110.2375].

[52] M. Hschele, J. Hoff, A. Pak, M. Steinhauser and T. Ueda, Comput. Phys. Commun. **185** (2014) 528 [arXiv:1307.6925].

[53] M. Hschele, J. Hoff, A. Pak, M. Steinhauser and T. Ueda, Phys. Lett. B **721** (2013) 244 [arXiv:1211.6559].

[54] T. Gehrmann and E. Remiddi, Nucl. Phys. B **601** (2001) 248 [hep-ph/0008287].

[55] D. Maitre, Comput. Phys. Commun. **174** (2006) 222 [hep-ph/0507152].

[56] E. Remiddi and J. A. M. Vermaseren, Int. J. Mod. Phys. A **15** (2000) 725 [hep-ph/9905237].

[57] A. B. Goncharov, Math. Res. Lett. **5** (1998) 497 [arXiv:1105.2076 [math.AG]].

[58] A. B. Goncharov, math/0103059 [math.AG].

[59] C. Duhr, H. Gangl and J. R. Rhodes, JHEP **1210** (2012) 075 [arXiv:1110.0458].

[60] H. Frellesvig, D. Tommasini and C. Wever, JHEP **1603** (2016) 189 [arXiv:1601.02649].

[61] C. W. Bauer, A. Frink and R. Kreckel, J. Symb. Comput. **33** (2000) 1 [cs/0004015].

[62] J. Vollinga and S. Weinzierl, Comput. Phys. Commun. **167** (2005) 177 [hep-ph/0410259].